What can we learn from AMMA about physical processes and models?

Françoise Guichard

CNRM (CNRS and Météo-France)

1. Broad context

AMMA stands for African Monsoon Multidisciplinary Analysis; it is "an international project to improve our knowledge and understanding of the West African monsoon (WAM) and its variability with an emphasis on daily-to-interannual timescales" (Redelsperger *et al.* 2006); further information can be found at http://science.amma-international.org/about/index.

An important motivation for AMMA is the major regional scale and multi-decadal West African drought. It started at the end of the 1960's, and was particularly severe in the seventies and eighties (Figure 1). It is indeed considered as the strongest observed event of rainfall variability at these time and space scales, and the actual mechanisms accounting for this drought are yet to be precisely determined (e.g.; Hulme 2001). In fact, modelling the West African weather and climate with current GCMs appear to be particularly difficult (Panareda *et al.* 2008, Hourdin *et al.* 2008). It is therefore not unexpected that climatic projections diverge widely over this region; Cook and Vizi (2006) for instance show how different ocean-coupled general circulation models (GCMs) predict either much drier or much wetter conditions over the Sahel for the twenty-first century.

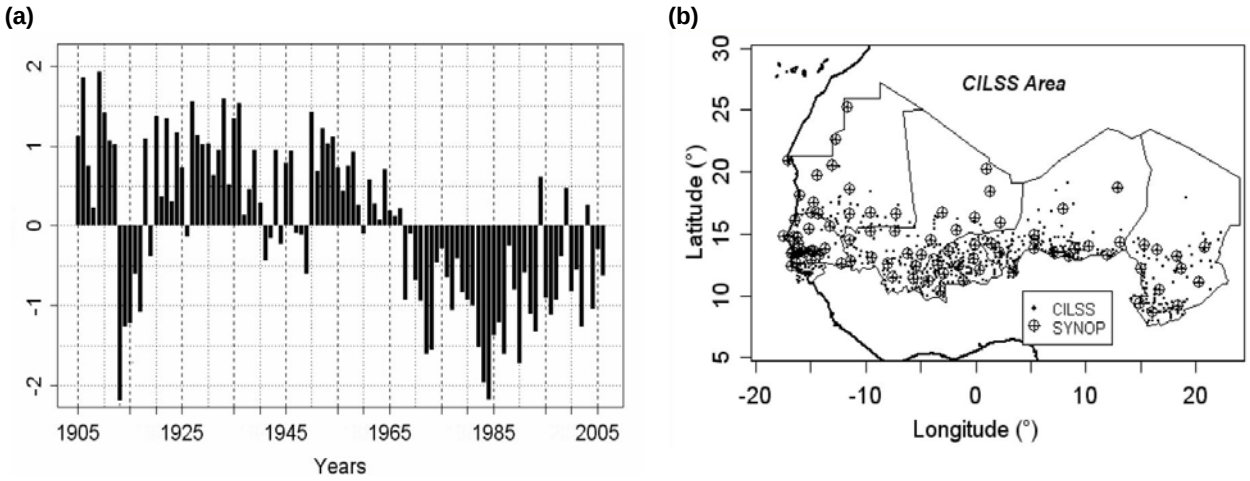

Figure 1, source Ali and Lebel (2008) :(a) Sahelian precipitation index (SPI) for the period 1905-2006; the SPI corresponds here to an arithmetic mean of normalized precipitation per year i from individual stations j, i.e. SPI(i) = Σ_j ($P_{i,j}$ - $<P_j>$) / σ_j , where $P_{i,j}$ is the annual rainfall for year i at station j, σ_j the standard deviation of annual rainfall at station j, and $<P_j>$ the average annual rainfall at station j, and (b) map of present rain gauges and SYNOP network.

As a result, the significance of conclusions that have been drawn from modelling approaches is sometimes limited. This probably contributes to the contrasting views found in the literature (e.g.; Charney 1975, Eltahir and Gong 1996). Indeed, datasets have been particularly limiting for testing the relevance of hypotheses or mechanisms put forward to account for various features of the West African monsoon. For instance, the role of *human-induced* changes on the variability of the land surface -and its consequences on the monsoon system- had been proposed as a major cause for the drought emphasized above. However, this view has been

much debated subsequently. It appears now that the reality involves more subtle modes of soil-surface-vegetation-atmosphere interactions (Taylor *et al.* 2002) as well as oceanic influences and climatic variability (Lamb 1978, Folland *et al.* 1986).

Physical and dynamical processes are strongly coupled within the West African monsoon. Therefore, *(i)* a better quantification of processes at play together with *(ii)* an identification of mechanisms and feedback loops actually operating, including their space and time scales, are probably central to advancing our understanding of this monsoon system.

In this respect, AMMA provides the first dataset documenting physical and dynamical processes on a range of time scales, from turbulent to inter-annual ones, along a pronounced meridional gradient, from the Gulf of Guinea to the Sahara, in a region where routine observations are notably sparse. In very short and incomplete, this includes: (a) a reinforcement of the existing network, notably for the soundings (Parker *et al.* 2008), *(b)* the installation for a few years of several ground-based stations (measuring in particular surface flux, precipitable water from GPS, aerosols properties), *(c)* an intensive observation period in 2006, when several aircraft, ships and ground-based radar were used, the frequency of soundings was enhanced, the ARM mobile facility was deployed in Niamey (Miller and Slingo 2007), among other instruments and platforms not listed here. This will allow us to conduct analyses of datasets, thus providing valuable guidance for model developments.

The importance of physical processes in the West African monsoon system implies that, in models, the parametrizations of these processes need to be explored in details. This includes interactions among them (e.g. surface, cloud and radiative processes) and couplings with the dynamics. In the past, such studies have been few, so that our knowledge is limited. On this modelling side, coordinated studies started within AMMA towards the assessment of models. Namely, this concerns land-surface modelling (ALMIP, Boone *et al.* 2008), the simulation of the water budget associated with convective systems in mesoscale models (Guichard *et al.* 2008a), and the seasonal cycle in climate models, including intraseasonal and synoptic modes of variability (AMMA-MIP, Hourdin *et al.* 2008, WAMME, Xue *et al.* 2008a).

Hereafter, I first present some important aspects of the West African monsoon system (section 2). In section 3, I summarize results from model intercomparisons; this helps providing an updated view on the capacities and limits of currently used modelling systems. Then, in section 4, I focus more precisely on processes involved in the water and energy cycles, as directly inferred from surface data in the Sahel. Such observational studies allow in particular to discriminate between mechanisms actually operating against existing hypotheses. Finally, in section 5, I conclude and present some perspectives regarding how AMMA can contribute to process studies and improvement of models in the future.

Note that results and discussions presented in sections 3 and 4 do not aim at covering the whole range of processes involved in the WAM system; they focus mainly on convection, cloud and radiative processes in relation to the surface water and energy budgets, and make use of material presented in Hourdin *et al.* (2008) (section 3.1), Guichard *et al.* (2008a) (section 3.2) and Guichard *et al.* (2008b) (section 4).

2. Basics features of the West African monsoon

It emerges from past research on the West African monsoon a significant but partial and composite knowledge, some elements of which are summarized below (and illustrated in the talk). Results from past experiments GATE (1974), COPT (1981), SEBEX (1990-1991), HAPEX-Sahel (1992) and JET2000 (2000) and related research stand out as important but separated steps in the building process of this knowledge.

At large scale, the area displays well defined and strong meridional gradients South of the Sahara. They are manifest on surface fields (rainfall, vegetation, albedo), as well as in the atmosphere above (e.g.; the African

Easterly jet developing in the Summer on the northern side of the rainbelt around 650 hPa, Thorncroft and Blackburn 1999, Cook 1999). These meridional features vary widely throughout the year (wet and dry seasons), and they display coupled seasonal and interannual fluctuations (Grist and Nicholson 2001) - see also Janicot *et al.* (2008) for an overview of the 2006 monsoon. This configuration inspired several modelling studies based on a zonally-symmetric modelling framework (e. g.; Zheng and Eltahir 1998, Peyrillé *et al.* 2007) and motivated the AMMA-CROSS project (Hourdin *et al.* 2008, briefly discussed below).

Then, the seasonal cycle is not smooth, i.e. intraseasonal variability is significant. For instance, the onset of the rainfall in the Sahel often takes the form of a fast "monsoon jump" during which the rainbelt is shifted some 5° northwards from its Spring location, at around 5°N along the coast of the Guinean Gulf. The depiction of this phenomenon is actually recent (Le Barbé *et al.* 2002, Sultan and Janicot 2003). Nevertheless, it can be noticed that such jump-like structures also characterizes other monsoon regions (e.g.; Lau and Yang 1996). More broadly, the mechanisms driving intraseasonal variability are not yet well understood. Recent studies have pointed to some role for the spatial configuration of the surface albedo (see Ramel et al. 2006), and for equatorial Kelvin and Rossby waves (e.g.; Matthews 2004).

At synoptic scale, atmospheric variability in Summer is dominated by African easterly waves (disturbances) travelling across West Africa (e.g.; Reed *et al.* 1977), and accounting at least partly for the large-scale organization of moist convection (this alone does not mean however that moist convection is simply *forced* by the dynamics of African easterly waves (AEWs)). These waves display a well defined signature in the meridional wind of the lower atmosphere; they are typically the strongest and the most coherent in September, a period during which Atlantic tropical cyclones have been shown to be associated with AEWs (Thorncroft and Hodges 2001). Their development had been initially related to the instability of the AEJ. However, recent studies, which consider more realistic background flows and examine the actual morphology of the waves, advocate other sources of AEW initiation (e.g.; Berry and Thorncroft 2005); they also emphasize interactions between waves and physical processes (Taylor and Clark 2001, Hsieh and Cook 2005). Thus, it appears that much is still to be understood regarding the nature of AEWs, their initiation, and more widely their entire life cycle (maintenance, splitting, merging, decay).

At mesoscale, attention has been paid to deep precipitating convection, but not so much to shallower clouds, nor to diurnal cycle issues. Over the region, moist convection can be very deep, with intense lightning activity. In the Sahel, this strength is not necessarily coupled to very high rainfall rates though, which points to the significance of rainfall evaporation. This is an area where long-lived spectacular mesoscale squall lines develop, accompanied by strong convective outflows sometimes materialized by lifted dust as haboobs (see talk, last page, middle photo). Mesoscale convective systems, taking or not the form of well defined squall lines, account for more than 70% of rainfall over this area (Mathon *et al.* 2022). This mesoscale organization of convection is nevertheless accompanied by a significant patchiness of surface rainfall down to scales on the order of ten kilometres. The nature of this patchiness is not well known, although observations provide evidence of positive soil moisture-rainfall feedbacks (Taylor and Lebel 1998).

Finally, on a wide range of space and time scales, the surface and low atmospheric levels are thought to be key elements of the West African monsoon (e.g.; Charney 1975, Eltahir and Gong 1996). However, the mechanisms of interactions actually operating between the surface and the overlying atmosphere are not well -and not all- known nor quantified. For instance, low-level mesoscale features were identified during JET2000 (Parker *et al.* 2005), but their significance in the WAM remains to be more fully explored. From the modelling side, the considerations above implies that particular care is required to simulate surface and boundary layer processes, and therefore, rainfall, vegetation, as well as clouds and aerosols, and likely convective outflows and falling rainfall evaporation.

3. Assessing current performances and limitations of models over West-Africa

3.1. At large scale

As pointed out in section 1, at regional scale, current coupled GCMs diverge particularly widely over West Africa. In such a modelling configuration however, errors in the ocean and in the ocean-atmosphere coupling can dominate over other sources of differences. This points to the need for alternative modelling frameworks. At large scale, three modelling projects have been set up, ALMIP, AMMA-MIP and WAMME (Xue *et al.*, 2008b); their first goal is to provide such adequate frameworks and to evaluate GCMs and land-surface models over West Africa.

Within AMMA-MIP for example, a "light but relevant framework to assess the model skill in terms of seasonal and intra-seasonal variations of West African monsoon" (Hourdin *et al.* 2008) had been set up as follows. SST have been prescribed, as it aims to evaluate more basic aspects of the simulation of the WAM at large scale. In practice, the focus is on the predominant dynamical structures such as the monsoon flow and AEJ, the rainfall belt, surface fluxes, and the mechanisms accounting for their simulation. As in Siebesma *et al.* (2004), a cross-section (a meridional one here), AMMA-CROSS is used for this purpose.

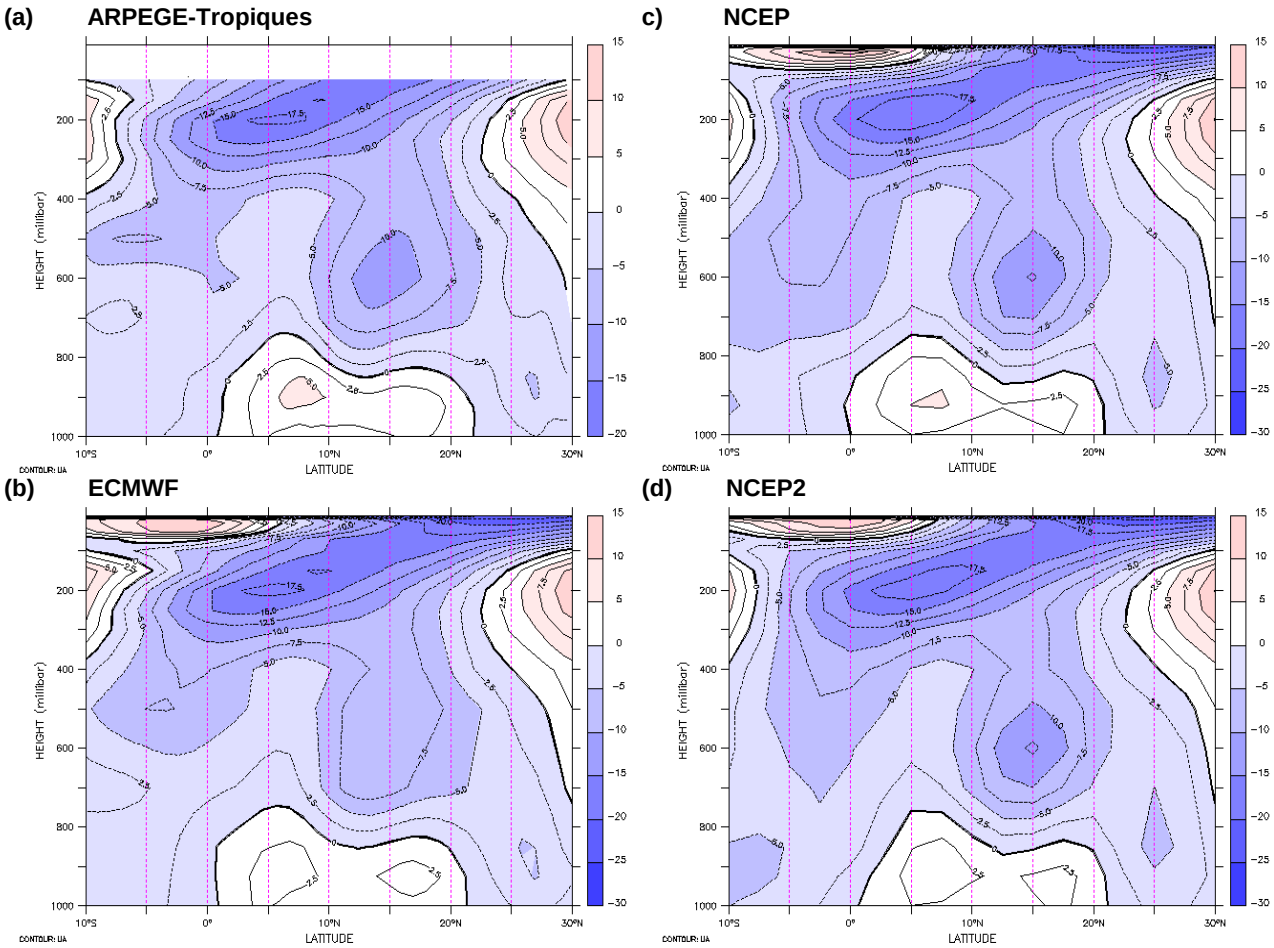

Figure 2 : Zonal wind during the core of the 2006 monsoon season (15 July-15 August) as a function of latitude, from 10°S to 30°N, and height on average over [10°W,10°E] from four meteorological analyses: (a) ARPEGE-Tropiques, (b) ECMWF, (c) NCEP and (d) NCEP2. Note that the relatively lower strength of the African Easterly jet (AEJ, around 15°N and 600 hPa) in the ECMWF compared to the other (re-) analyses around 15°N is related to the absence of the 600 hPa level in the available pressure grid.[figures prepared by F. Favot]

It appears that current NWP (re-)analyses are valuable to assess some of these features, although not all of them. Namely, they provide relatively close pictures of zonal circulations and intraseasonal fluctuations (Figure 2), but not of meridional wind and vertical velocity (Figure 3), nor of rainfall, or surface and TOA energy fluxes.

For instance, the AEJ location (latitude and height) and strength are very close among (re-)analyses, while the basic characteristics of the low-level monsoon flow such as its meridional extend, height and strength are more contrasted. Note that some of the differences in the AEJ are likely explained by differences in available vertical grids (coarser versus finer, see legend of Figure 2).

However, the summer rainbelt is not well positioned in NWP products: it is shifted to the South by a few degrees in the ECMWF-IFS compared to surface-based and satellite rainfall estimates (Panareda *et al.* 2008), this is also the case in the NCEP reanalysis.

Satellite products also show a well defined tropical tongue of maximum TOA net radiative flux ($R^{net,TOA}$) reaching the Sahel in Summer (Figure 3, top right). The surface energy balance over land implies that $R^{net,TOA}$ provides an estimate of the net energy input to the atmospheric column below (assuming a negligeable ground heat flux). High $R^{net,TOA}$ values are indicative of regions where convection, either dry or moist, is thermodynamically favoured (Chou and Neelin 2003). Over West Africa, the high $R^{net,TOA}$ tongue arises from a particular combination of season-varying surface and cloud radiative properties in both the longwave and shortwave. Furthermore, meridional contrasts in cloud radiative properties are responsible for

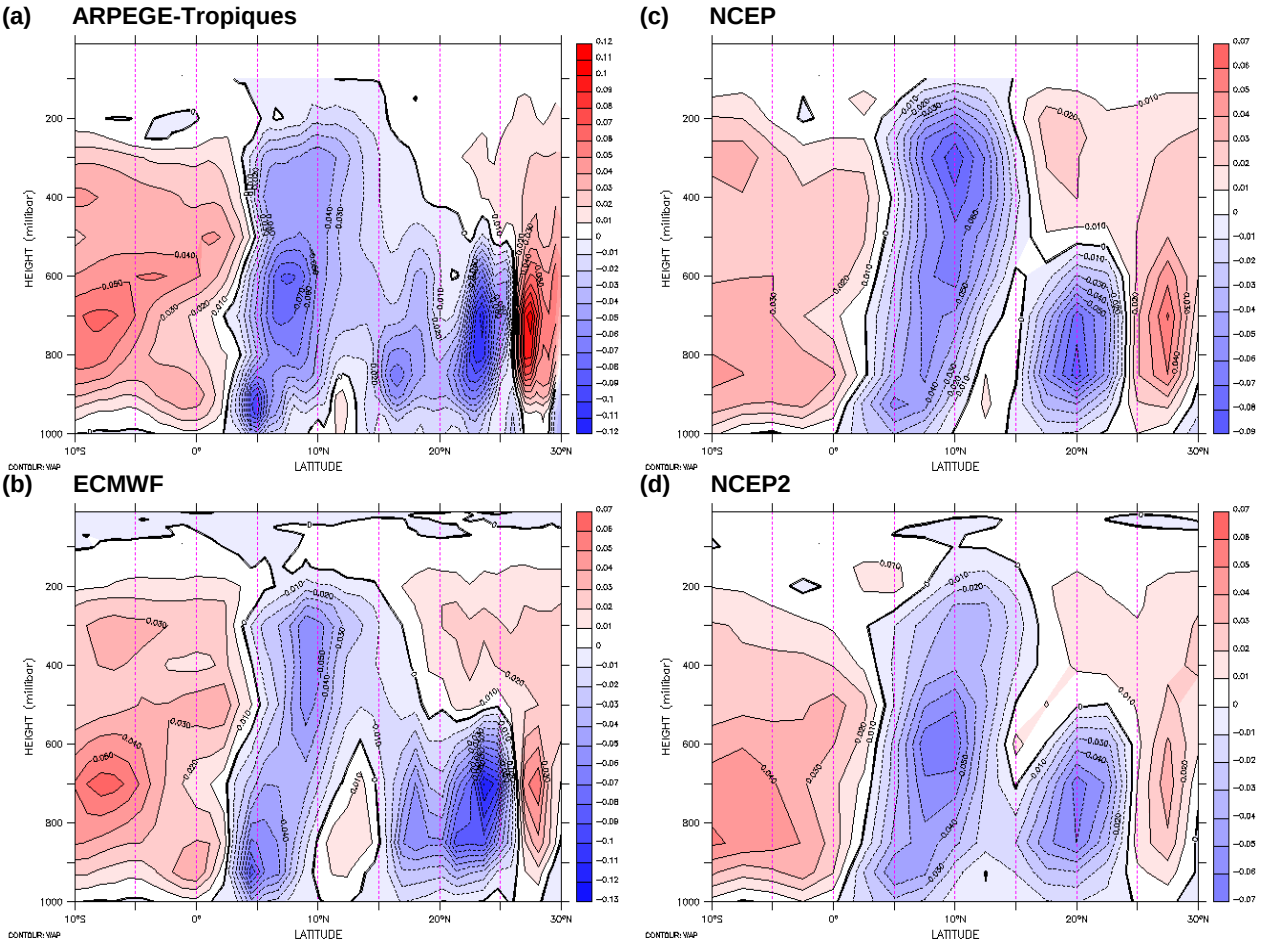

Figure 3 : Same as Figure 2 except for vertical velocity. North of 20°N, the differences in the strength of the horizontal gradients below 600 hPa are partly due to the differences in the horizontal interpolation grids (0.5° in ARPEGE-Tropiques, 1.125° in ECMWF, and 2.5° in NCEP and NCEP2).[figures prepared by F. Favot]

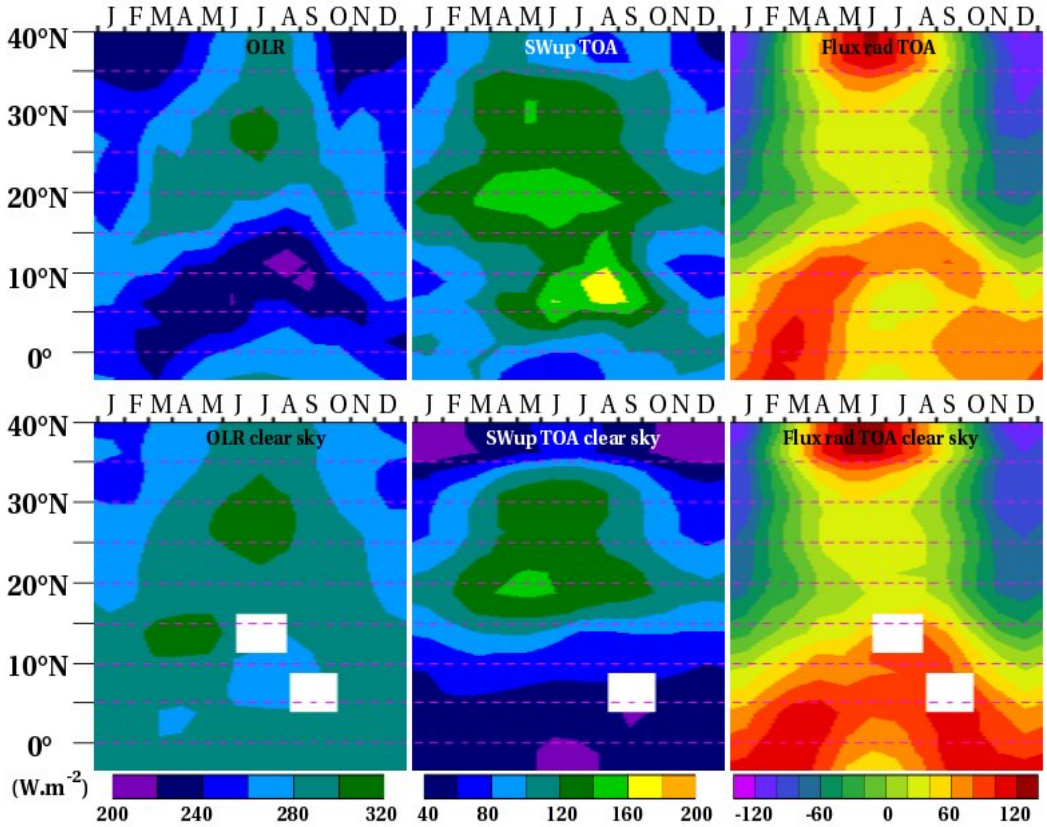

Figure 4: Satellite estimate of time-latitude series of radiative fluxes at the top of the atmosphere (top) and their associated clear sky estimates (bottom), the outgoing longwave radiation (left), upward shorwave flux (middle) and net radiative flux (right) are presented – from CERES-TERRA 2003 monthly-mean values with a spatial resolution of 2.5°, contour interval is 20 W.m^{-2}.[figures prepared by F. Favot]

the northward shift of this tongue (Figure 2, top right and bottom right). The significance of this delicate TOA energetic feature needs to be investigated further. However, it is currently not well captured by most NWPs, as a result of too approximate surface and TOA fluxes.

Several climate models participate to this ongoing AMMA-MIP project. They are generally able to simulate a monsoon flow and an AEJ over West Africa, but they display large spread already in their zonal circulations, and wide differences in their rainbelts and magnitudes of intraseasonal variability. These large-scale features do not seem to involve a significant role for model internal sources of variability. On the other hand, they show a strong sensitivity to physical parametrizations. For instance, the AEJ disappeared when changing the parametrization of moist convection in the LMD climate model (see Hourdin *et al.* 2008 for more details). A full understanding of the different mechanisms operating in these models and an assessment of their relevance is still to be gained, but observations collected within AMMA will contribute to reach this goal.

3.2. At mesoscale

Large-scale models do not capture properly some basic characteristics of moist convection such as its diurnal cycle and mesoscale organization; this is the case over West Africa (WA) as well (e.g.; Lebel *et al.* 2000). On the other hand, the simulation of MCSs over WA with mesoscale modelling showed more success (Diongue *et al.* 2002). Within AMMA, modelling studies focused on the water cycle are currently carried out. One of the objectives of the study summarized below was to compare the simulation of an observed MCS, its associated rainfall and surface evapotranspiration as obtained from different mesoscale models (see Guichard *et al.* 2008a for more details).

It appears that initial and boundary conditions, which in the present case are provided by an analyse, significantly control the location of the simulated rainfall field at synoptic scales for 1-2 day forecasts (in case of strong AEW activity at least). Indeed, the use of initial and boundary conditions derived from different analyses leads to fairly distinct simulations of large-scale patterns in convection and rainfall for otherwise identical configurations of a mesoscale simulation.

On the other hand, when different mesoscale models are initialized and forced at their boundaries by the same analysis (from ECMWF in the present case), they are able to simulate a propagating rainfall feature that crosses a broad area [0°W-10°E,7°N-16°N] (Figure 5), as estimated from high frequency satellite rainfall products (Figure 6, upper panel), and as also simulated by the ECMWF-IFS (Figure 5, bottom left). This occurs even though several of these mesoscale simulations made use of a horizontal resolution coarser than 10 kilometres and therefore made use of a parametrization for the representation of deep precipitating convective processes.

The differences in rainfall rates between the two satellite estimates (illustrated in Figure 6 underlines the difficulty encountered with currently available data and algorithms. Nevertheless, both satellite products indicate the same timing and propagation speed of the rainfall feature (compare Figure 6 left and right panels). Such an agreement is not found in mesoscale simulations. The simulated propagating rainfall feature does not depart so much in terms of its speed, but it is usually not precisely located within the area delineated by the two blue curves. This reflects a problem of timing. In addition, significant rainfall rates are often forecast at other locations. Another issue is the difficulty to simulate the path followed by the rainfall feature along latitude (Figure 7). For this case, both satellite estimates indicate a northward propagation (Figure 6, lower panel), while mesoscale simulations diverge widely, especially at nighttime, when rainfall is shifted Southwards in many cases.

Simulated surface evapotranspiration (E) fields are also found to vary significantly among mesoscale models, in terms of magnitude and meridional gradients, and much more so than estimates provided by different land surface models (LSMs) used in an offline mode (ALMIP, Boone *et al.* 2008). A major difference between these two estimates is the rainfall field and surface incoming radiative flux "seen" by the LSM: in offline simulations, observational products are used (satellite based estimates). In the present case, a common weakness of the simulated evapotranspitation fields is their lack of zonal asymmetry, compared to ALMIP estimates. In some models, it is associated with a large overestimation of E, of about 20% for 24h-mean values over an area more than 1000 km wide. A comparison of surface energy budgets implies that these differences are not explained by differences in the evaporative fraction. They are in fact related to different surface net radiative fluxes. The latter is in turn linked to much higher surface incoming solar radiative fluxes in the mesoscale simulations. This points to a lack of cloudiness in these simulations, and implies a large impact on daytime boundary layer at synoptic spatial scales, in terms of growth (height) and water vapour amount in particular.

This too approximate depiction of surface fluxes, involving feedbacks on -and from- other physical processes, probably play a role in the fast (one to a few days) drifts affecting mesoscale simulations of monsoonal circulations (e.g.; Söhne *et al.* 2008), as previously highlighted in NWPs by (Thorncroft *et al.* 2003, see also Tompkins *et al.* 2005).

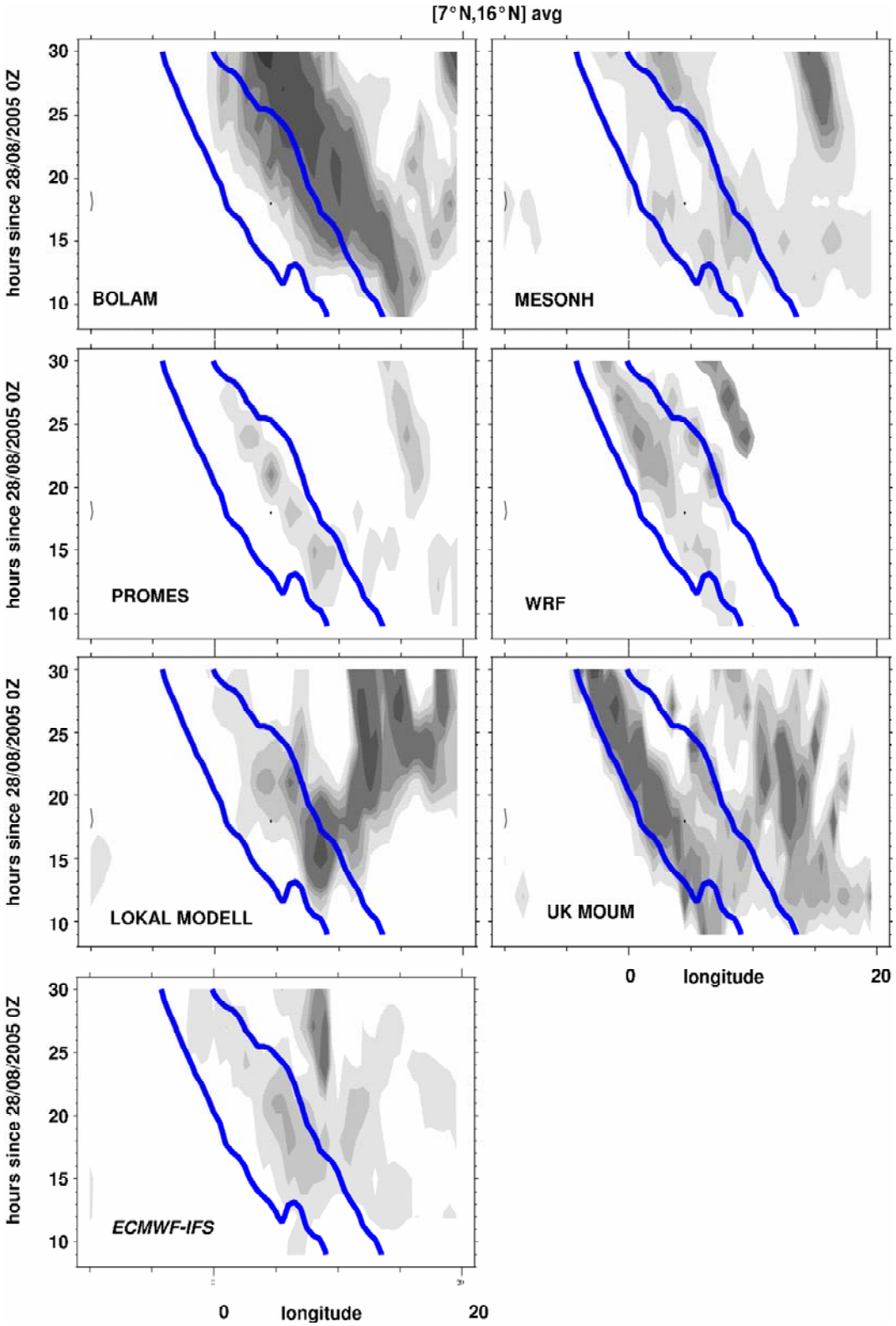

Figure 5: Longitude-time diagrams of simulated surface rainfall, averaged over [7°N,16°N], grey shadings for values from 1, 2, 3, 4, 5, 10, 15, 20 mm and above; the blue thick lines delineate the areas where the satellite rainfall estimate (EPSAT-SG) is greater than 2mm (3-hourly cumulative values).

The choice of a higher, 'deep-cloud-resolving', resolution (less than 5 km) is found to affect the simulation in the following ways: spatio-temporal distributions of rainfall and surface heat fluxes display more variability at scales of a few tens of kilometres, the simulated MCS propagates somewhat faster, and its trajectory is shifted northwards (compare Figure 8(a) and (b)). The seemingly close distributions of daily

cumulative rainfall (Figure 8(c), dotted lines) involves compensations between the rainfall patterns at smaller time scale and the propagation as can be inferred from 3-h cumulative rainfall distributions (Figure 8(c), solid lines). These differences involve quantitative changes in simulated processes, which result in part from differences in their couplings. As an example, for this case-study, rainfall in the coarser-grid simulation, using a parametrization of convection, develops earlier in the day, in response to an increase in CAPE (Guichard *et al.* 2004); the CAPE increase itself is related to the daytime increase of boundary layer equivalent potential temperature in the present case. This affects an area several hundreds of km wide, but does not generate much cloud cover, so that this early day surface wetting is followed by an enhanced daytime evapotranspiration. The scenario will probably vary from one model to the other, as it relies heavily on the functioning of a convection scheme, in particular its triggering criteria, but also on a cloud scheme and the parametrization of their interactions.

In summary, this section emphasizes how the representation of physical processes is key to the simulation of numerous features of the West African monsoon on a range of space and time scales. Conversely, from another perspective, it shows how the West African monsoon corresponds to a very rich test bed for process studies and for the development of physical parametrizations.

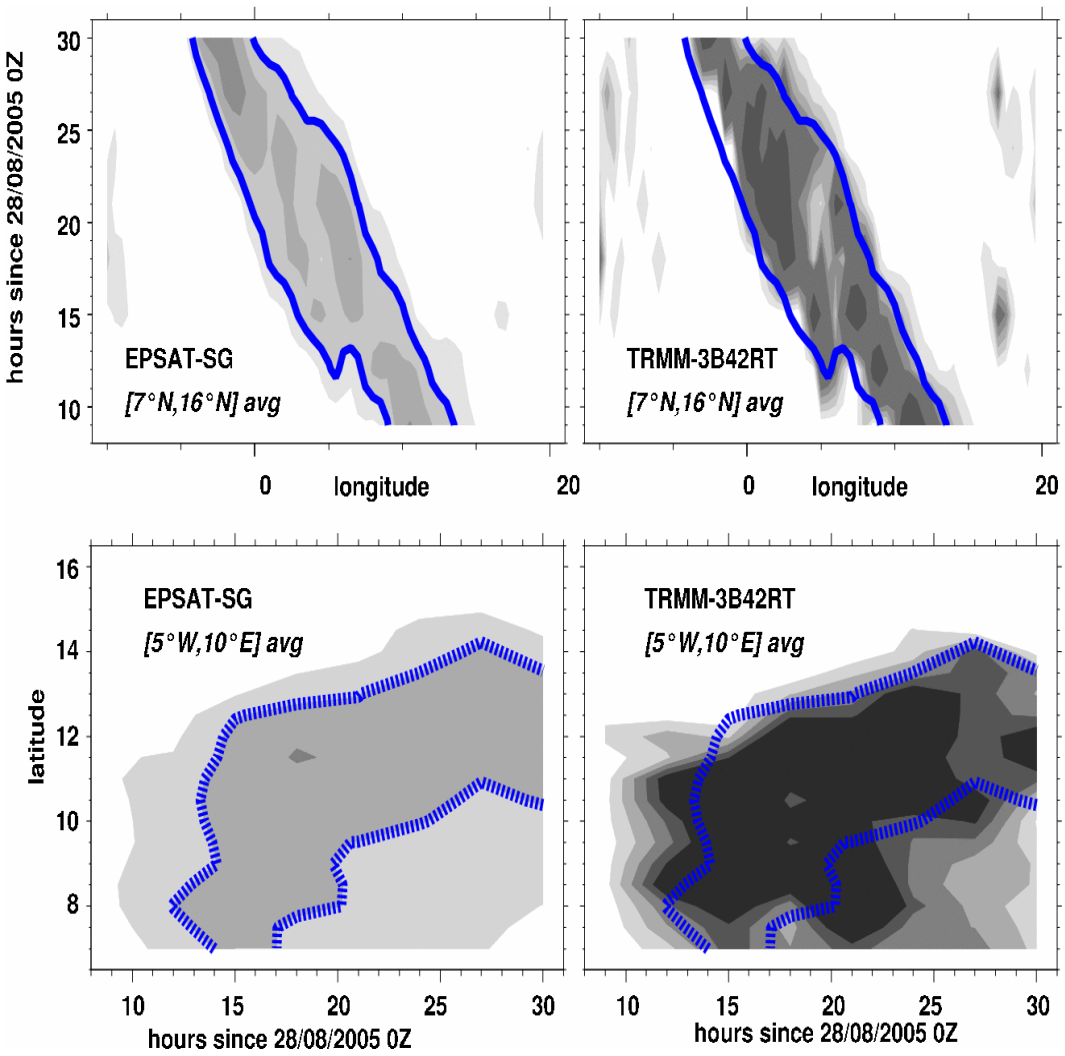

Figure 6 Longitude-time (top) and time-latitude (bottom) diagrams of two distinct satellite estimates of surface rainfall, 3-h cumulative value averaged respectively over [7°N,16°N] and [5°W,10°E], grey shadings for values from 1, 2, 3, 4, 5, 10, 15, 20 mm and above, EPSAT-SG (left) and TRMM-3B42RT (right); the blue thick lines delineate the area where the EPSAT-SG rainfall estimate is greater than 2 mm - values are affected respectively at the end (the centre) of the 3-hourly intervals for EPSAT-SG (for TRMM-3B42RT).

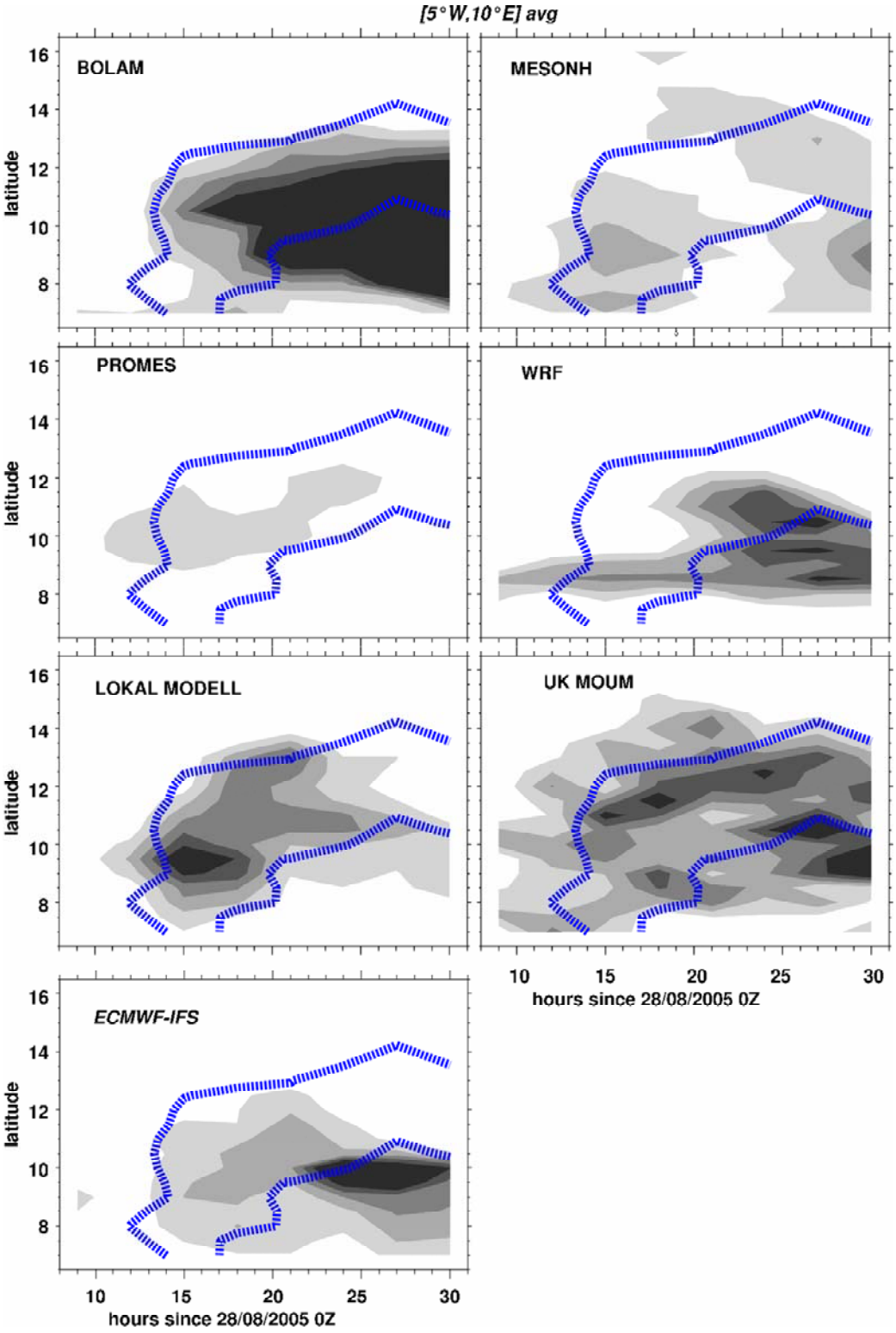

Figure 7: Time-latitude diagram of simulated surface rainfall, averaged over [5°W,10°E], grey shadings for values from 1, 2, 3, 4, 5, 10, 15, 20 mm and above; the blue thick lines delineate the area where the EPSAT-SG rainfall estimate is greater than 2mm (3-h cumulative values).

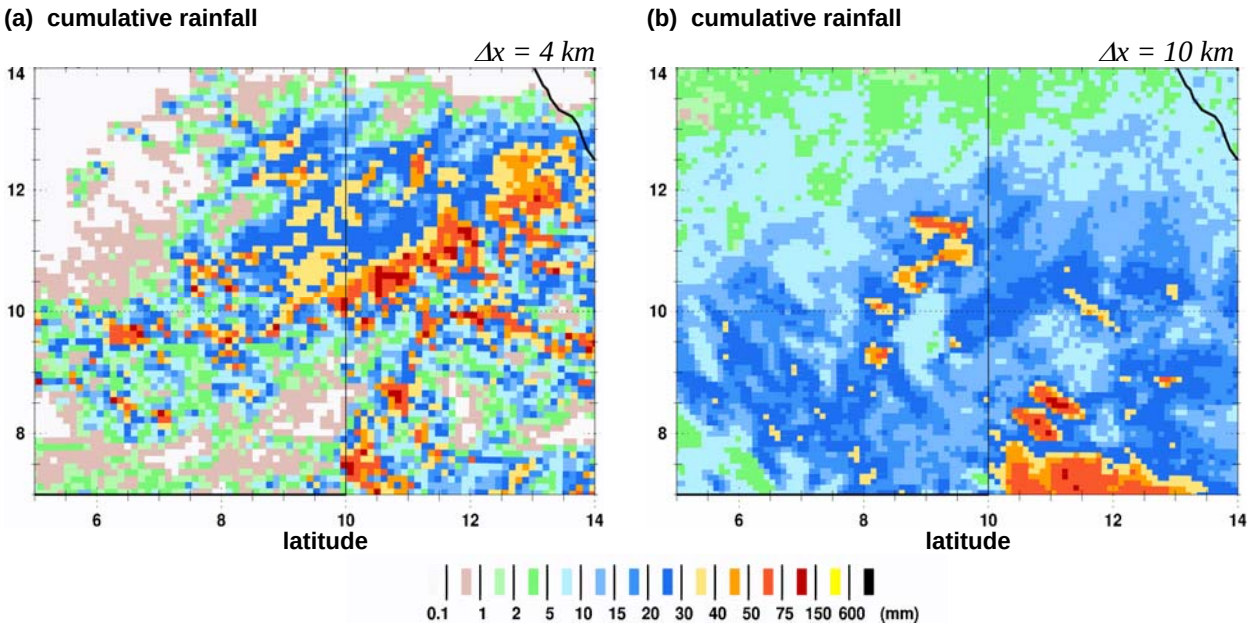

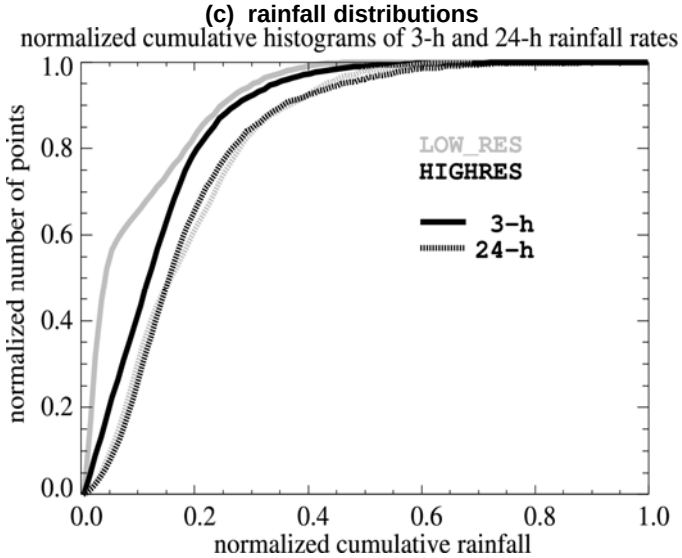

Figure 8: Simulated cumulative rainfall from early morning (6Z) to midnight using (a) a higher horizontal resolution (4 km) without parametrization of convection and (b) a lower horizontal resolution (10 km) with a parametrization of convection. (c) presents the normalized distributions of 3-h (solid lines) and 24-h (dotted line) cumulative rainfall over the spatial domain shown in (a),(b) for the two simulations, with higher (black) and lower (grey) resolution – (mesoNH simulations from N. Asencio).

4. Sahelian surface thermodynamics and radiative budget

Previous sections emphasize the importance of surface energy fluxes in the WAM. Data collected within AMMA allow exploring this issue further. They provide guidance for modelling. This is illustrated below with results from Guichard *et al.* (2008). It addresses the issue of the factors controlling surface net radiation, and their coupling with surface meteorological data. Multi-year high-frequency surface data collected in the Sahel are well suited for such studies. They point to radical differences but also similarities of this semi-arid continental surface with other mid-latitude and tropical land regions (e.g.; Betts and Ball 1998, Betts *et al.* 2002). Hereafter, data presented are from an automatic weather station located in Agoufou, at [1°W, 15°N], within the Malian Gourma, in a grassland over sandy soil, which is the dominant surface type in this area. Departure of the ECMWF-IFS from these data is also briefly discussed.

4.1. Major features

In the Sahel, the contrast is sharp between dry conditions prevailing from October-November to April-May and the moist summer months. This is illustrated in Figure 9 with time series from 2003. The area is the coldest around December, then a sustained heating takes place from January to May. From May until October, the monsoon flow is well established, but the majority of rainfall events take place only between June and September (vertical bars in Figure 9). Specific humidity at 2m AGL (q) increases progressively from May until August, while the low-level monsoon flow actually weakens during the same period, in both speed and depth (Figure 10). Thus, the rainy core of the monsoon season (August, day of year 213 to 244) does not coincide with the period during which the low-level south-westerly flow is maximum. This probably involves *(i)* the weaker dynamic influence of the Saharan heat low which moves northwards and westwards in Summer, and *(ii)* changes in the vertical extend of turbulent mixing between the low-levels and the atmosphere above between June (over a dry bare soil) and August (over a wet vegetated surface). Finally, a fast drying and heating takes place in October when the monsoon flow retreats.

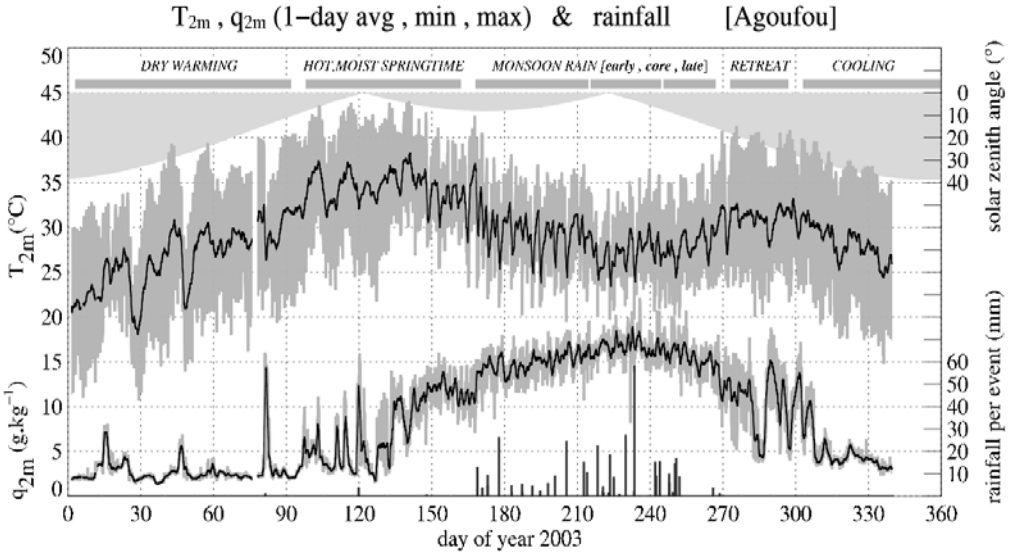

Figure 9 : Time series of 2-m temperature (upper curve) and specific humidity (lower curve) in 2003 (the black lines correspond to a 24-h running mean and the dark grey shadings delineate 24-h minimum and maximum values), rainfall amounts per rainy event (bottom bars) and midday solar zenith angle (light shading). - different time periods are roughly delimited by the top thick grey lines with names given above.

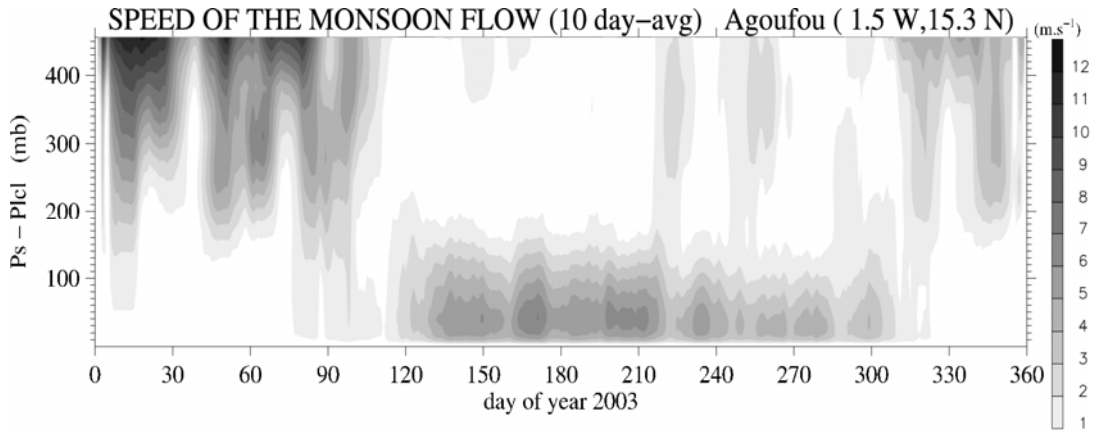

Figure 10: Time-height series of wind speed in the "monsoon flow" - ECMWF analysis for the column above the measurement site, using a 10 day-running mean; only positive zonal and meridional components of the wind have been retained; the vertical axis is the surface pressure minus pressure height.

A striking feature of the Sahelian surface climate is the strong dynamics associated with the transition from a drier hot Spring to a brief cooler moist tropical Summer climate (Figure 9). It also involves large transformations of the diurnal cycles of thermodynamic, dynamic and radiative fields. In particular, for all moist Summer months except August, specific humidity decreases in such a way during daytime (Figure 11a) that it prevents an afternoon increase of the equivalent potential temperature θe (Figure 11b). For instance in June, q decreases by more than 2g.kg^{-1} between 8Z (equivalent to local solar time here) and 14Z, and θe actually decreases slightly after 10Z despite the daytime temperature increase. In fact, the diurnal cycle of θe is almost flat in June. This also leads to large daytime drops of relative humidity, which enhances the daytime rise of the lifting condensation level *lcl* (Figure 11c) - *lcl* is expressed here as the departure, in mb, from surface pressure, noted *Ps-Plcl* ; this cloud-base estimate can also be considered as a proxy for the mixed layer height in case of a *cloudy* convective boundary layer (see the seminar lecture by A. K. Betts for a comprehensive explanation on the strong correlation between relative humidity and the *lcl*).

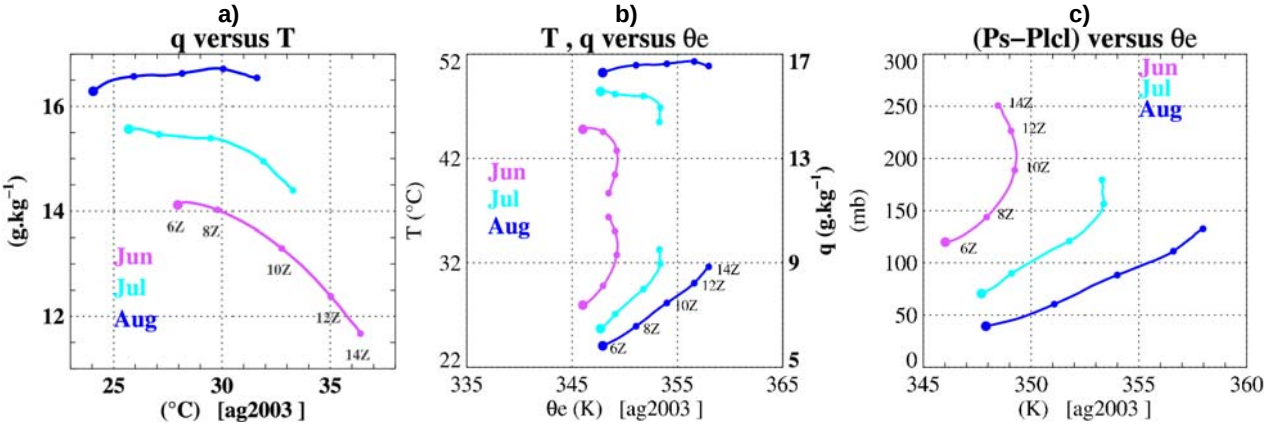

Figure 11: monthly-mean daytime variations (6Z to 14Z) of the couplets (a) [q,T], (b) [T,θe] and [q,θe], and (c) [Ps-Plcl ,θe] in June (pink), July (cyan) and August (blue).

At the surface, seasonal variations of surface net radiation, R^{net} (Figure 12) are also large. For the year considered, 2003, it increases progressively from around 20 W.m^{-2} (for 10-day mean values) at the coldest of the dry season, until May, when it reaches around 60 W.m^{-2}. It increases more sharply after the onset of rainfall, up to 160 W.m^{-2} in late August. The following decrease is fast, and lasts until December. This well-

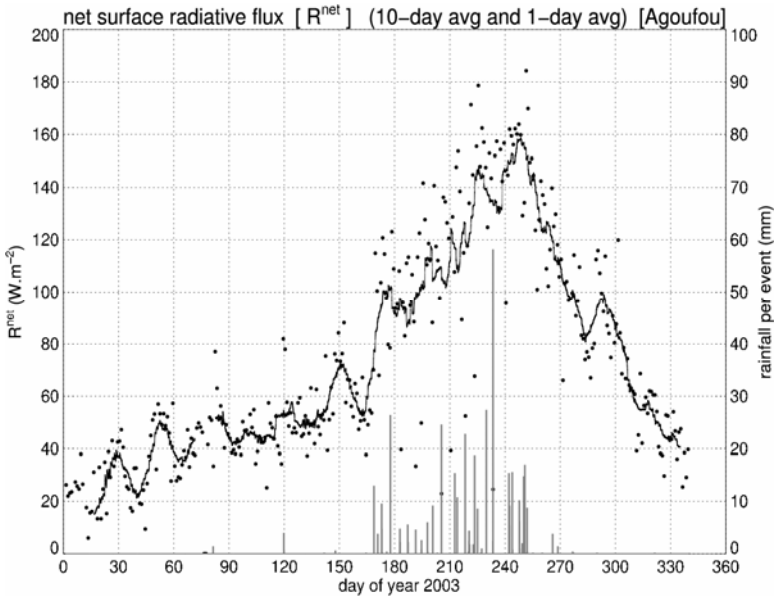

Figure 12: Time series of surface net radiation (R^{net}) and rainfall per event (bottom bars) in 2003, the black line corresponds to a 10-day running mean and the dots to 24-h average values.

defined pattern results nevertheless from a subtle combination of changes in surface incoming and upwelling shortwave and longwave fluxes (R^{net} = SW^{in} - SW^{up} + LW^{in} – LW^{up}). These changes results surface and atmospheric processes which are differently coupled throughout the year. They emphasize the continental nature of this tropical semi-arid area, as presented below.

4.2. Surface radiative budget

Firstly, the seasonal cycle of R^{net} is not simply related to SW^{in}, and the seasonal fluctuations of SW^{in} in turn depart significantly from the seasonal cycle of the incoming solar radiation at the top of the atmosphere (TOA) (Figure 13, upper curve). Note that, given the latitude of the Sahel, two minima of the solar zenith angle (SZA) are recorded within the year - above the site, the TOA incoming solar flux displays its maximum in May, but it does not changes much until the second SZA minimum, around mid-August. At the surface, SWin also increases from January to early May, but then weakens sharply until mid-June. The departure of SWin from the solar incoming radiation at the TOA involves changes in humidity, but also a significant radiative forcing by clouds and aerosols. At the surface, they are found to account for a reduction of the incoming shortwave flux of about 25% in July-August, which corresponds roughly to 80 $W.m^{-2}$. This result points to the need of an accurate modelling of the cloud field, even for such a semi-arid area.

The solar radiation reflected by the surface, SW^{up}, does not follow the seasonal evolution of SW^{in} (Figure 13, middle curve), as it is shaped by the seasonal cycle of both SWin and surface albedo (Figure 13 lower curve), discussed in more details by Samain et al. (2008). The consistent negative trend developing throughout the monsoon season (higher than 0.1 in 2003) is linked to the growth of the vegetation, which is darker than the bright sandy surface. Rainfall events also induce albedo drops reaching up to 0.1 (the sand is darker when wet), but they are short-lived (1-2 days). Therefore, this effect is enhanced when rainfall events are more numerous, and when the vegetation cover is low.

The longwave upward flux, LW^{up} (Figure 14, upper curve) and surface air temperature (Figure 9, upper curve) display similar seasonal evolutions, with two maxima, in Spring and Autumn, two minima, in Winter and Summer, and a weakening of their diurnal ranges in Summer (grey shading). As the surface warms up, from January until mid-May, LW^{up} increases steadily. Then, from mid-May until the end of August, LW^{up} decreases, in two steps.

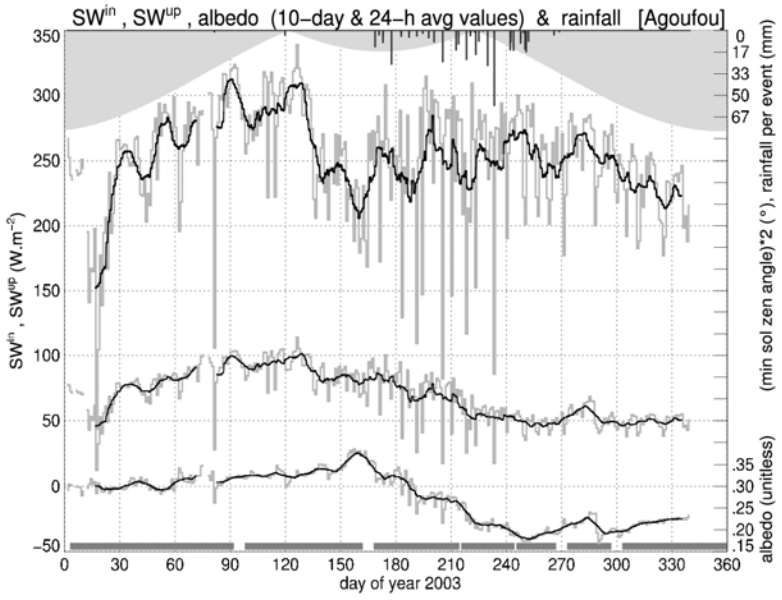

Figure 13: Time series of surface surface shortwave incoming (SW^{in}, upper curve), shortwave upwelling (SW up, middle curve) and albedo (lower curve, right y axis); the thick black line corresponds to a 10-day running mean and the thin grey line to 24-h average values - upper black bars indicate rainfall events.

In a first step, once the monsoon flux becomes established, LW^{up} decreases very slightly until the first significant rainfall event, a few weeks later, in June (days of year 135 to 165). This arises from a much weaker *daytime* surface longwave emission, linked to reduced insolation (Figure 13), which more than compensates for the positive jump of nighttime LW^{up}, associated with a weaker nocturnal cooling (Figure 9). In a second step, after the first significant rainfall event until the end of July, LW^{up} decreases sharply in response to rainfall events, by several tens of $W.m^{-2}$ each time. As the albedo, LW^{up} also increases back rapidly after rainfall. Finally, in August, LW^{up} remains low, mostly because of its daytime reduction. The response to rainfall events is less dramatic than in July, with LW^{up} overall lower than before.

Finally, the surface downward longwave flux LW^{in} displays large seasonal fluctuations, but again along another path (Figure 14, lower curve). LW^{in} is much lower during the colder months and much higher from May to September during the moist months. From January to May and October to December, its synoptic fluctuations closely match those of precipitable water (see Guichard et al. 2008). However, from January to April (*dry warming months*), they are superimposed to a larger-scale positive trend mirroring the steeper trend of LW^{up},(Figure 14, upper curve) until the sharp jump of LW^{in} at the arrival of the monsoon flow. Thus, LW^{in} is maximum from mid-May to mid-June, i.e., once the monsoon flux is established, but prior to the onset of rainfall, when the atmosphere is quite warm, moist and aerosol loaded. In fact, from April to Mid-June, LW^{in} fluctuations closely match those of $-SW^{in}$ (Figure 13, upper curve).

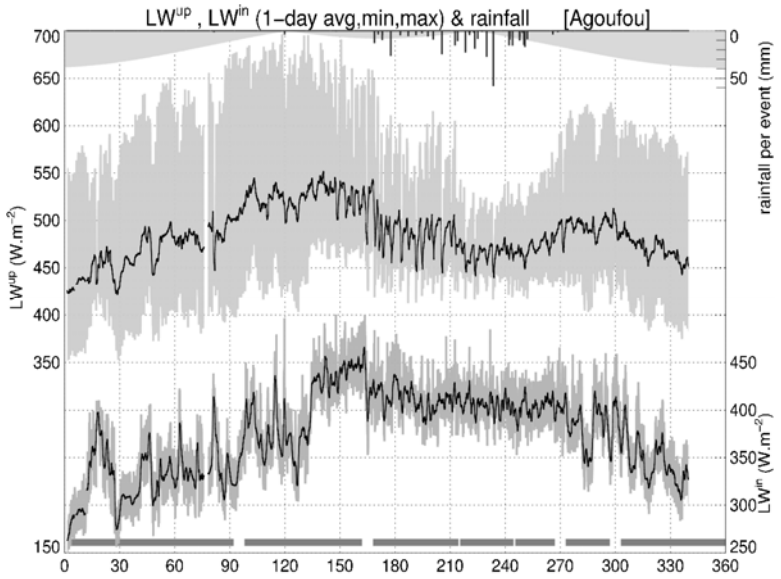

Figure 14: Same as Figure 9 except for surface longwave fluxes, LW^{up} (upper curve) and LW^{in} (lower curve).

Regarding this Spring moistening period prior to rainfall, it implies:

(1) a daytime warming of the optically thicker atmosphere at the expense of the surface,

(2) a partial balance of this daytime process by the nighttime downward radiative emission of the now warmer atmosphere (LWin increases), consistent with the higher nighttime surface LW emission and temperature at 2m.

As a result, from late May until the first rainfall event, LW^{up} and surface air temperature decrease, but only slightly.

Then, day to day variations of LW^{in} are weak until September. Nevertheless, the negative trend of LW^{in} taking place throughout the monsoon season is astonishing. It occurs despite the increase of precipitable

water from June to August and likely involves an overall cooling of the atmosphere as a whole operated by the monsoon phenomenon.

The partition of R^{net} into surface longwave and shortwave radiative fluxes (LW^{net} and SW^{net}) highlights how, from January until the first rainfall event, LW^{net} and SW^{net} almost cancel each other (Figure 15(a)). This reflects a low capacity of the coupled surface-atmosphere system to efficiently trap the top of the atmosphere increasingly high solar influx, until the atmosphere becomes moist. Indeed, as emphasized by Betts (2004) for other regions, in this semi-arid Sahelian location as well, fluctuations of daily-mean LW^{net} and moisture are strongly linked all year long (Figure 16(a)). In this figure, the lifting condensation level is used as the moisture variable: a lower height of the *lcl* - or alternatively a higher relative humidity - is associated with higher surface LW^{net}, across the whole range of humidity fluctuations.

The shortwave-longwave partition used above does not provide a simple explanation for the seasonal evolution of R^{net} though. Another partition consists in splitting the radiative budget into incoming and upwelling fluxes. Then, the negative LW^{in} and positive SW^{in} trends happen to partly cancel each other during the moist Spring and Summer months, so that their sum, R^{in} does not changes much during this period. Therefore, the enhancement of R^{net} mostly reflects changes of surface properties that arise in relation with the monsoon, and results from changes of both LW and SW surface upwelling radiative fluxes (Figure 15(b)). Thus, R^{net} can efficiently increase only within a narrow time window, shifted by about two months with respect the TOA incoming radiative flux, a window further restricted in time by the retreat of the monsoon flow and fast increase of LW^{up} after the last rain.

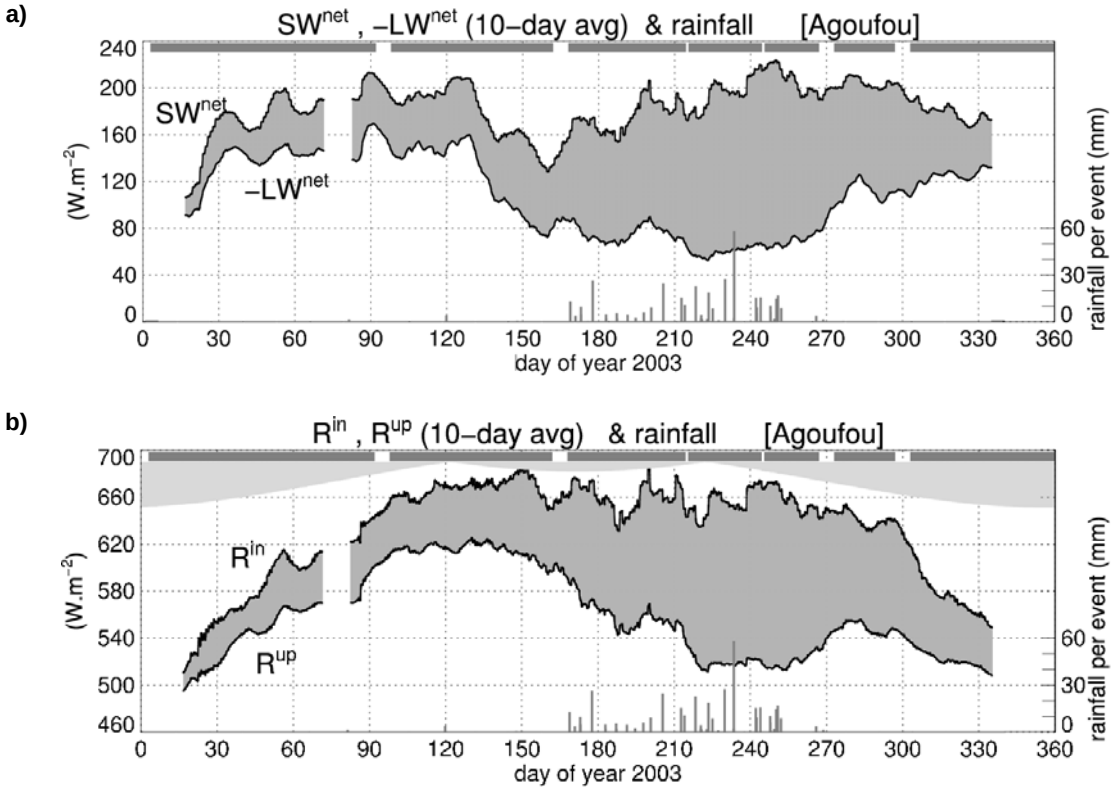

Figure 15: Time series of 10-day mean surface (a) net SW and LW fluxes (black curves), note that the lower solid line corresponds to ' - LW^{net} ', so that the the grey shaded area enclosed within the two black curves gives the magnitude of the surface net radiation R^{net} , (b) incoming radiative flux (R^{in} = SW^{in} + LW^{in} , upper black line) and outgoing radiative (R^{up}= LW^{up} + SW^{up}, lower black curve) - lower black bars are rainfall per event (right y axis).

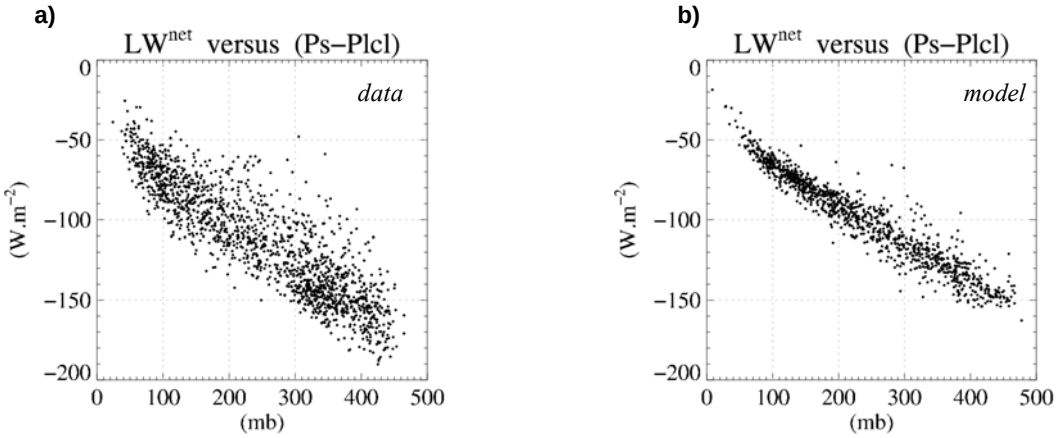

Figure 16: Scatter diagram of daily mean LW^{net} versus (Ps-Plcl), (a): observations, data from 2002 to 2007 (single location) and (b) ECMWF-IFS.

4.3. Surface thermodynamic-radiative coupling during the monsoon

A synthetic view of specific couplings encountered during the monsoon season is shown in Figure 17.

LW^{net} was previously found to be strongly linked to the *lcl* (Figure 16(a)). R^{net} is found to increase even more than LW^{net} as *lcl* decreases (Figure 17(a)). This feature is explained by the semi-arid nature of the area, where the reduction of the incoming solar radiation by the cloud cover and aerosols is lower than other sources of variations of R^{net} (namely surface longwave emission and albedo). The few heavily cloudy days account for the scatter obtained at lower R^{net} values (cf dots in Figure 12 and upper grey curve in Figure 13). On the other hand, θe overall increases under moister and colder conditions, i.e. when the height of the *lcl* decreases (Figure 17(b)), and the co-variation of their 24-h mean values still involves the co-variation of their diurnal cycle and its changes along the Summer (Figure 11(c)).

Thus, both θe and R^{net} increase at lower *lcl* heights (Figure 17(a,b)) and are found to be positively related (Figure 17(c)). This result is *broadly* consistent with previous studies which have related low-level moist static energy to soil-moisture through consideration of the surface energy balance (e.g.; Eltahir 1998). However, in the present case, it arises via a distinct interplay among processes. The strong and fast increase of R^{net} along the monsoon season is mostly explained by the surface cooling and darkening (vegetation growth), while the increase of θe involves a strong lowering of mixed layer height (*lcl*) associated with cooler moister conditions in the low levels, and large change in diurnal cycles. In fact, the surface incoming LW flux is not *increasing* but *decreasing* as the atmosphere becomes moister and cloudier (Figure 14, lower curve). Furthermore, the cloud shortwave radiative impact is found to be significant (several tens of $W.m^{-2}$); nevertheless, from June to August, SW^{in} displays a positive trend (Figure 13, upper curve), involving a weakening of the aerosol radiative impact.

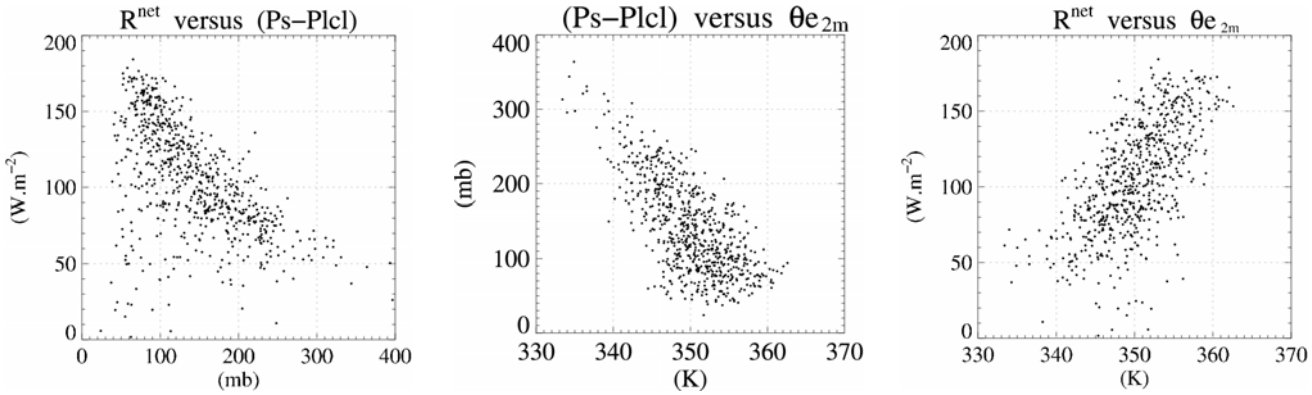

Figure 17 : Scatter diagrams of (a) R^{net} versus (Ps-Plcl), (b) (Ps-Plcl) versus θe and (c) Rnet versus θe.

It is important to note that the seasonal cycle discussed above made use of data from a *good* monsoon year; i.e. with ample rainfall. Over the Sahel however, interannual variability of rainfall is known to be strong, from larger to smaller scales. For instance, in 2004, the rainfall amount was less than half its value of 2003 (185 against 430 mm) locally in Agoufou. The discussion above suggests that a more rainy monsoon will also be characterized by higher surface net radiation. Indeed, variability of R^{net} from one Summer to the next is found to be strong. This is illustrated in Figure 18. The differences are the strongest in Summer. For instance, R^{net} differs by almost 30 $W.m^{-2}$ on average between August 2003 and August 2004. The interannual variability of R^{net} is also largely explained by changes in surface properties as emphasized above. It involves the vegetation dynamics, which accounts for large interannual fluctuations of albedo (Samain *et al.* 2008). However, processes accounting for LW^{up} interannual variability are found to be at least as important. As mentioned above, LW^{up} decreases sharply in response to rainfall events. At larger time scale, LW^{up} and rainfall are also found to be strongly linked (not shown).

Overall, these results emphasize the *strong couplings of the energy and water cycles* taking place in the Sahel over a wide range of scales, and including also aerosols and vegetation-related processes. From a modelling side, they also help identifying the important processes at play, how they interact, when and at which scales. This provides guidance over an area where such interactions are complex, and not all complying to existing conceptual schemes.

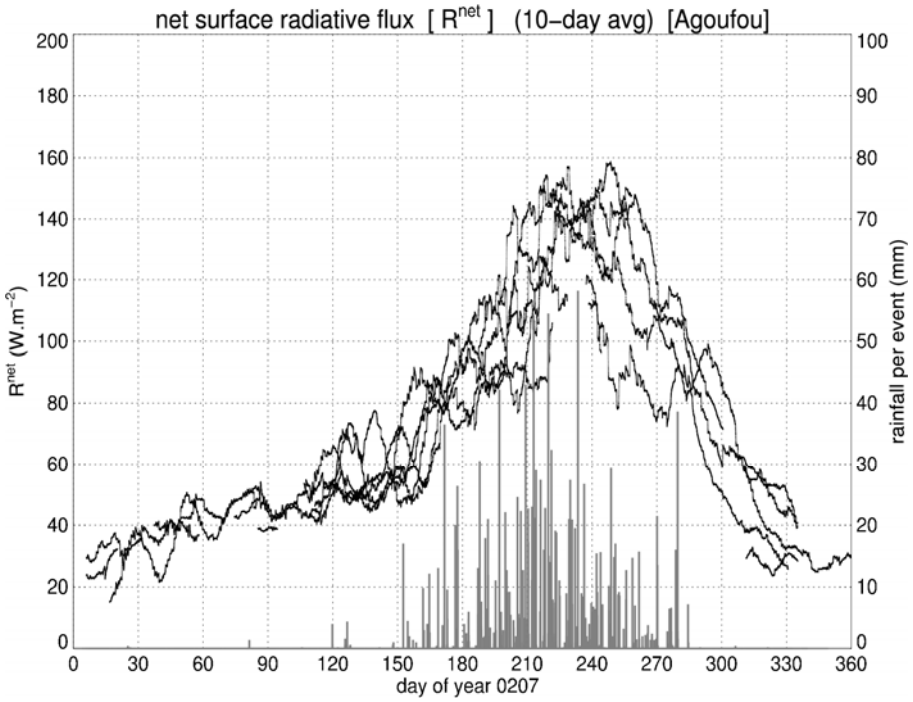

Figure 18: Same as Figure 12 except for the 10-day average time series covering 2002 to 2007.

4.4. Modelling the surface radiative budget

Modelling the surface radiative budget appears as particularly challenging in view of the major role played by physical processes in shaping this budget. This is illustrated here with a few results from the ECMWF-IFS, where the closest model grid point is examined (it corresponds to a horizontal area on the order of 35 x 35 km^2). Obvious limitations to such an exercise include some differences in the simulated and observed surface properties. For instance, the model albedo, which is based on prescribed albedo maps, remains higher than observed in Summer (albeit not in 2004, a particularly *bad* monsoon). Nevertheless, some important differences are already highlighted in this way. For the area considered, they appear to concern a larger spacial scale than only this local measurement site.

Figure 19 compares time series of observed (red) and simulated (blue) surface 10-day mean R^{net} in 2003. The amplitude of the simulated seasonal cycle of R^{net} is almost as large as observed, but shifted earlier in time by more than a month. On the other hand, rainfall events are frequently simulated (light blue bars) but cumulative rainfall is very weak for most of them. This is related to the difficulty of the ECMWF-IFS to simulate rainfall in the Sahelian band (Panareda *et al.* 2008). However, the two stronger rainfall events are followed by an exaggerated, strong and long lasting, response in surface radiative fluxes and thermodynamics (not shown), visible as a drop in R^{net} centered around day of year 220 in Figure 19(a). It is explained by a large reduction of R^{in} exceeding a coupled R^{up} decrease (Figure 20(b)). Compared to data (Figure 20(b)), R^{in} and R^{up} are more strongly coupled in the model.

Simulated rainfall did not improved since 2003 (it actually appears to be slightly lower), but the R^{net} maximum has been shifted in time to August in more recent simulations (Figure 19(b)). This feature seems to be related to the change of the aerosol climatology in October 2003 as reported in Tompkins *et al.* (2005). Nevertheless, the Spring to early Summer R^{net} is now higher than observed. This difference is not limited to one particular Sahelian site but concerns all the AMMA measurements sites, from the Soudanian zone around 9°N to the Northern fringe of the Sahel at 17°N.

Prior to the onset of rainfall, it is chiefly explained by a larger incoming shortwave flux (see illustrations in the talk), which points to a lack of clouds and/or aerosols (in 2003, the excessive aerosol optical thickness had perhaps compensated for this lack of cloudiness). During the core of the monsoon season, at the Sahelian sites where the simulated rainfall is too low, the overestimation of SW^{in} is partly balanced by both too high SW^{up} and LW^{up} (this is reflected in their sum R^{up}, see lower curve in Figure 20(d) compared to Figure 20(c)), LWin is also found to be usually slightly higher (not shown).

This behaviour consistent with a simulated atmosphere being warmer, over a simulated surface where enhanced sensible heat flux generates higher drier and less cloudy convective boundary layers than observed. It seems unlikely that aerosols alone account for the differences noted in August; however, they probably play a more important role in Spring and early Summer.

Finally, in the simulation also, LW^{net} and *lcl* are strongly coupled (Figure 16(b)). In Agoufou, LW^{net} does not reach values as low as observed, at high Plcl, corresponding to dry surface air. The simulation of nighttime turbulent mixing could contribute to such a difference (e.g.; being weaker than simulated). However, similar comparisons for other Sahelian sites do not support this “single-process” hypothesis and suggest that more subtle explanations are needed.

Overall, such comparisons point to first order deficiencies in models. In the present case, beyond an improvement of surface schemes (notably their representation of vegetation), they also emphasize the need for a better representation of surface rainfall, cloud cover and aerosols. For instance, it seems difficult for this model (and for other models not presented here), to simulate sharp-enough variations of surface radiative fluxes occurring prior to and around the Monsoon onset. Thus, the significance of the underlying processes for this onset, if any, would not be well captured anyway.

5. Conclusion and perspectives

West Africa is a region where modelling is very challenging, and for which improved parametrizations are critically needed. The unprecedented large amount of data collected during the AMMA 2006 field campaign will help advancing on these issues in several ways. It already contributed to provide (re)analyses of a quality that was probably never reached in the past over this data-sparse region (Panareda and Beljaars 2008), thanks in particular to the ‘reactivation of the radiosonde network over West Africa’ (Parker *et al.* 2008). Regarding processes involving atmospheric moisture, the development of suitable methods for the

correction of humidity bias affecting different sounding types (Nuret *et al.* 2008, Panareda *et al.* 2008) also contributes to this enhanced quality.

At large scale, it appears that a framework such as AMMA-CROSS, inspired by the approaches of Siebesma *et al.* (2004) and Peyrillé *et al.* (2007), is a useful tool over this continental area (Hourdin *et al.* 2008). Firstly, it constitutes an efficient way to assess the simulation of major large-scale features of the West African monsoon (monsoon flow, jets, rainbelt...). Secondly, it provides a valuable diagnostic tool for testing the impacts of new or modified parametrizations. In this respect, models of intermediate complexity such as two-dimensional zonally-symetric models (e.g.; Zheng and Eltahir 1998, Peyrillé *et al.* 2007) could prove complementary. They offer a link between simpler single-column models in which feedbacks between physical and dynamical processes are limited by design and more complex three-dimensional GCMs.

On the other hand, the relationships observed between physical processes and synoptic structures such as African Easterly waves cannot be *directly* addressed with such a 2D methodology. From phenomenological as well as theoretical perspectives, AEWs are still the object of numerous investigations. In terms of model evaluation, within AMMA-MIP, high-frequency series of horizontal maps documenting both the surface and different atmospheric layers are currently exploited to advance on this important topic (Hourdin *et al.* 2008).

Finally, extensive comparisons of analyses, re-analyses and satellite products help delineating better their limits and usefulness for assessing large-scale models. They must be used with great caution regarding large-scale vertical velocity fields, but also the atmospheric low levels and surface fields.

In the future, large-scale modelling will also benefit from AMMA in other ways. For instance, improved (re)analyses and estimations of surface fluxes (e.g.; ALMIP, Boone *et al.* 2008) certainly provide a closer depiction of the reality than available previously. Long-term surface-based datasets can also be used in statistical ways to explore and to assess coupling mechanisms arising on different scales.

In addition, as in GATE, COARE and a few other field campaigns, it will be possible to estimate atmospheric budgets from the multi-day high-frequency sounding network set up in 2006. Notably eight soundings were release each day at five locations, during two multi-day periods. In the past, such datasets proved to be quite useful, and for very long, regarding the development of parametrizations. It should also be the case for this dataset documenting a new continental tropical climate of the globe.

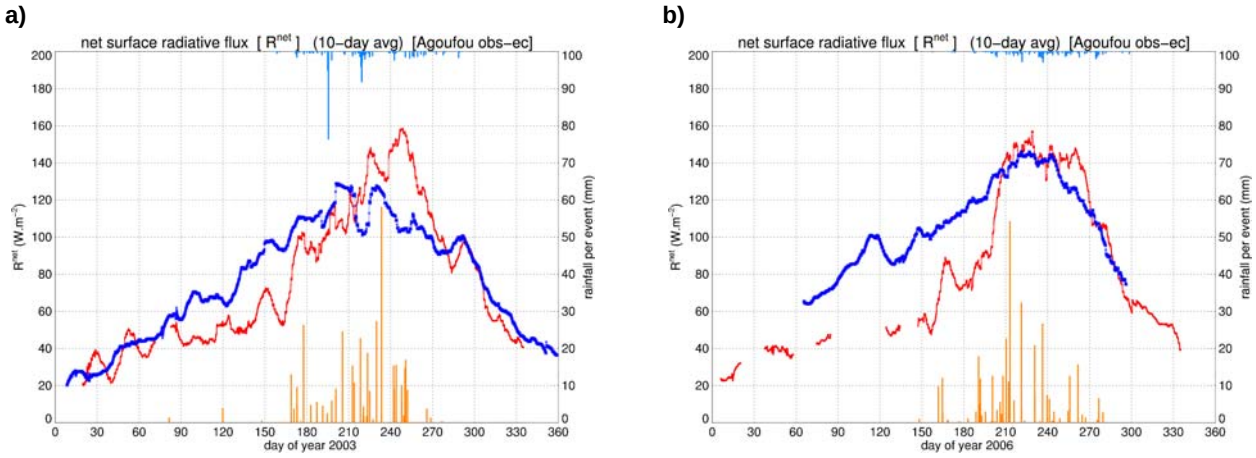

Figure 19: (a) Same as Figure 12 except showing both data and model in 2003, with red line (resp. blue line) for 10-day mean R^{net} and orange bottom bars (resp. light blue top bars) showing rainfall per event, (b) same as (a) except for 2006.

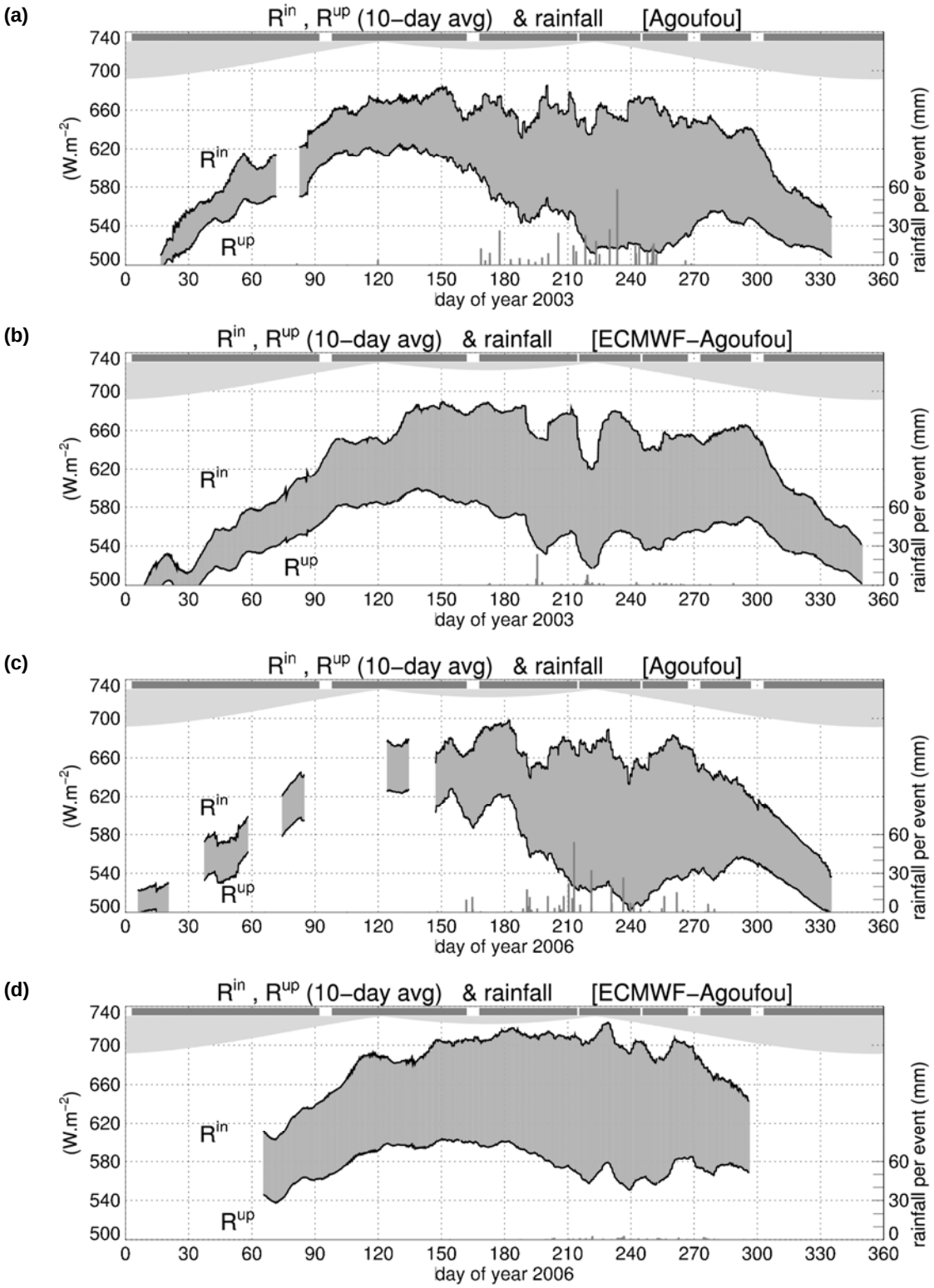

Figure 20: (a) same as Figure 15 except for a 40W.m^{-2} shift in y-axis, (b) same as (a) except for the model and (c,d) same as (a,b) except in 2006

On another side and scale, mesoscale models have some capacity to simulate propagating rainfall systems, even though numerous and various difficulties are still affecting regional mesoscale modelling, e.g.; crudeness of current surface and cloud initialization methods, diurnal cycle issue... However, the utilization of a fine-resolution in such simulations (on the order of a few kilometres, i.e. able to capture deep convective cells) can lead to radically different representations of processes down to scales of a few tens of kilometres.

More analyses is needed in order (1) to assess the quality of such simulations, this can be done on the basis of AMMA case-studies for which relevant observations are available; and (2) to quantify the processes and to precisely identify the mechanisms operating within these simulations. In this context, CRMs and LES can be seen as useful complementary tools, as they are well suited for basic process and sensitivity studies. For instance, they would be helpful for identifying the effective couplings involved in the development of convective phenomena over arid and semi-arid areas.

Finally, observations collected within AMMA provide a basis for numerous, valuable, process studies. They allow advancing our knowledge, which is still limited and composite over West Africa. Therefore, they provide important guidance rather than simply a mean to evaluate models.

This was illustrated in section 4 with a quantitative analysis of the surface radiation budget for a representative Sahelian site (Guichard *et al*. 2008b), recalling here the importance of surface fluxes to several aspects of the West African monsoon. It shows that the Summer increase of surface net radiation is strong and largely driven by modifications of the surface via rainfall events and vegetation phenology (surface cooling and darkening), while the *direct* impact of atmospheric changes on the total incoming radiation is limited to shorter time scales.

Subtle balances between surface air temperature and moisture fields are found on a range of scales. For instance, during the monsoon, apart from August, their opposite daytime fluctuations (warming, drying) lead to an almost *flat* diurnal cycle of the low-level equivalent potential temperature θe. This feature stands out in contrast to other less arid continental regions. More broadly, the strong dynamics associated with the transition from a drier hot Spring to a brief cooler wet tropical Summer climate involves large transformations of the diurnal cycles, even within the monsoon season. The particular combination of thermodynamic and radiative variations taking place during the monsoon eventually leads to a positive correlation between θe and R^{net}. This correlation is, in turn, broadly consistent with an overall positive soil-moisture rainfall feedback at this scale.

Observations further reveal astonishing radiative signatures of the monsoon on the incoming longwave flux at the surface. In particular, LW^{in} does not reach its maximum during the monsoon season when the atmosphere is the most cloudy and humid, but earlier, prior to the onset of rainfall, as the dry and *warmer* atmosphere suddenly becomes moist. Conversely, the incoming solar radiation at the surface increases slightly from late Spring to the core monsoon season even though the atmosphere becomes moister and cloudier; this possibly involving a high aerosol optical thickness in late Spring early Summer.

Beyond these Sahelian-specific features however, and in agreement with some previous studies, strong links are found between the atmospheric humidity and the net longwave flux at the surface all year long, even across the much lower humidity ranges encountered in this region. They point to and locally quantify the major control of water vapour and water-related processes on the surface-atmosphere thermal coupling as measured by LW^{net}. Namely, they are found to be more tightly coupled (LW^{net} closer to 0) when the atmosphere is moister (and cloudier).

Observational results such as presented above provide valuable ground truth for assessing models over a continental area displaying a rich variety of surface-atmosphere regimes throughout the year, from a desert-like to a rainy tropical-like climate during the core of the monsoon. This was illustrated briefly with results from the ECMWF-IFS. In summary, it appears that the parametrization of cloud and rainfall processes still constitute major sources of errors in the surface energy budget, through their impact on the surface incoming solar radiation and evaporative fraction. In addition, changes in the physics of a model (in the present case a modification of the aerosol climatology) can dominate interannual variability of the surface energy budget.

A more accurate and renewed picture of the West African monsoon system is beginning to emerge from process studies carried out within AMMA. The degree to which each physical parametrization, taken separately, should be improved for an adequate modelling of the WAM is not always clear. However, a satisfactory representation of their mutual interactions and couplings with dynamical processes appears as a crucial issue, across a wide range of space and time scales. The West African monsoon thus provides a valuable test bed for physical parametrizations, particularly over continental areas. As such, it should also contribute to improve modelling over other regions.

Acknowledgements

I thank my colleagues who participated to the studies presented above, especially F. Favot, F. Hourdin and I. Musat (section 3.1), N. Asencio, O. Bock, C. Peugeot and J.-L. Redelsperger (section 3.2), and P. Hiernaux, L. Kergoat, E. Mougin and F. Timouk (section 4).

References

Agustì-Panareda A., and A. Beljaars, 2008. ECMWF's contribution to AMMA. ECMWF Newsletter 115, http://www.ecmwf.int/publications/newsletters/pdf/115.pdf.

Agustì-Panareda, A, D. Vasiljevic, Anton Beljaars, O. Bock, F. Guichard, M. Nuret, A. Garcia Mendez, E. Andersson, P. Bechtold, A. Fink, H. Hersbach, J.-P. Lafore, J.-B. Ngamini, D. J. Parker, J.-L. Redelsperger and A. Tompkins, 2006: Radiosonde humidity bias correction over the West African region for the special AMMA reanalysis at ECMWF. submitted to *Quart. J. Roy. Meteor. Soc.*

Ali, A., and T. Lebel, 2008: The Sahelian standardized rainfall index revisited. *Int. J. Climatology*, to appear.

Berry, G. J., and C. Thorncroft, 2005: Case study of an intense African easterly wave. *Mon. Wea. Rev.*, 133, 752-766.

Betts, A. K., and J. H. Ball, 1998: FIFE surface climate and site-average dataset 1987-89. *J. Atmos. Sci.*, 55, 1091-1108.

Betts, A. K., J. D. Fuentes, M. Garstang and J. H. Ball, 2002: surface diurnal cycle and boundary layer structure over Rondônia during the rainy season. *J. Geophys. Res.*, 107(D20), 8065.

Betts, A. K., 2004. Understanding hydrometeorology using global models. *Bull. Atm. Met. Soc.*, 85, 1673-1688.

Boone, A., P. de Rosnay, G. Balsamo, A. Beljaars, F. Chopin, B. Decharme, C. Delire, A. Ducharne, S. Gascoin, F. Guichard, Y. Gusev, P. Harris, L. Jarlan, L. Kergoat, E. Mougin, O. Nasonova, A. Norgaard, T. Orgeval, C. Ottlé, I. Poccard-Leclercq, J. Polcher, I. Sandholt, S. Saux-Picart, C. M. Taylor, and Y. Xue, 2008: The AMMA Land Surface Model Intercomparison Project (ALMIP). submitted to *Bull. Amer. Meteor. Soc.*

Charney, J.G., 1975: Dynamics of deserts and drought in the Sahel. *Quart. J. Roy. Meteor. Soc.*, 101, 193-202.

Chou C., and J. D. Neelin, 2003: Mechanisms Limiting the Northward Extent of the Northern Summer Monsoons over North America, Asia, and Africa. *J. Climate*, 6, 406–425.

Cook, K. H., 1999: Generation of the African easterly jet and its role in determining West African precipitation. *J. Climate*, 12, 1165-1184.

Cook, K. H., and E. K. Vizy, 2006: Coupled Model Simulations of the West African Monsoon System: Twentieth- and Twenty-First-Century Simulations. *J. Climate*, 19, 3681–3703.

Diongue, A, J.-P. Lafore, J.-L Redelsperger and R. Roca, 2002: Numerical study of a Sahelian synoptic weather system: Initiation and mature stages of convection and its interactions with the large-scale dynamics. *Quart. J. Roy. Meteor. Soc.,* 128, 1899-1927.

Eltahir, E. A. B., 1998. A soil moisture–rainfall feedback mechanism, 1, Theory and observations. *Water Resour. Res.*, 34, 765–776.

Eltahir, E. A. B. and C. Gong, 1996: Dynamics of wet and dry years in West Africa. *J. Climate*, 9, 1030–1042.

Folland, C. K., T. N. Palmer, and D. E. Parker, 1986: Sahel rainfall and worldwide sea temperature 1901-1985. *Nature*, 320, 602-607.

Grist, J. P., and S. E. Nicholson, 2001: A study of the dynamic factors influencing the rainfall variability in the West African Sahel. *J. Climate*, 14, 1337–1359.

Guichard, F., J. C. Petch, J.-L. Redelsperger, P. Bechtold, J.-P. Chaboureau, S. Cheinet, W. Grabowski, H. Grenier, C. J. Jones, M. Koehler, J.-M. Piriou, R. Tailleux and M. Tomasini, 2004: Modelling the diurnal cycle of deep precipitating convection over land with CRMs and SCMs. *Quart. J. Roy. Meteor. Soc.*, 130, 3139-3172.

Guichard F., N. Asencio, C. Peugeot, O. Bock, J.-L Redelsperger, X. Cui, M.-A. Gaertner, M. Garvert, B. Lamptey, E. Orlandi, J. Sander, M. Zampieri, A. Boone, F. Fierli, S. Jones, et al., 2008a: Simulations and observations of rainfall and evapotranspiration associated with a mesoscale convective event over West Africa. to be submitted to *Wea. For.* (for now AMMA-EU D1.2.2.b deliv. report)

Guichard, F., L. Kergoat, E. Mougin, F. Timouk, F. Baup, P. Hiernaux and F. Lavenu , 2008b: Surface thermodynamics and radiative budget in the Sahelian Gourma: seasonal and diurnal cycles, *J. Hydrology*, AMMA special issue, in press.

Hourdin, F., I Musat, F. Guichard, P. Ruti, F. Favot, M.-A. Filiberti, M. Pham, J.-Y. Grandpeix, A. Dell'Aquila, P. Marquet, H. Gallee, T. Losada Doval, A. Traore, J.-P. Lafore and J-.L. Redelsperger, 2008: The AMMA-Model Intercomparison Project. submitted to *Bull. Amer. Meteor. Soc.*

Hsieh, J.S., and Cook K. H., 2005: Generation of African easterly wave disturbances: Relationship to the African easterly jet. *Mon. Wea. Rev.*, 133, 1311-1327.

Hulme, M., 2001: Climatic perspectives on Sahelian dessication: 1973-1998. *Global Environmental Change* 11, 19-29.

Janicot, S., C. D. Thorncroft, A. Ali, N. Asencio, G. Berry, O. Bock, B. Bourles, G. Caniaux, F. Chauvin, A. Deme, L. Kergoat, J.-P. Lafore, C. Lavaysse, T. Lebel, B. Marticorena, F. Mounier, P. Nedelec, J.-L. Redelsperger, F. Ravegnani, C. E. Reeves, R. Roca, P. de Rosnay, H. Schlager, B. Sultan, M. Tomasini, A. Ulanovsky1, and ACMAD forecasters team, 2008: Large-scale overview of the summer monsoon over West Africa during the AMMA field experiment in 2006. *Ann. Geophys.*, 26, 2569-2595.

Lamb, P. J., 1978: Large-scale tropical surface circulation patterns associated with Subsaharan weather anomalies. *Tellus*, 30, 240-251.

Lau, K.-M., and S. Yang, 1996: Seasonal variation, abrupt transition, and intraseasonal variability associated with the Asian Summer monsoon in the GLA GCM. *J. Climate*, 9, 965-985.

Lau, K. M., S. S. P. Shen, K. M. Kim and H. Wang, 2006: A multimodel study of the twentieth-century simulations of Sahel drought from the 1970s to 1990s. *J. Geophys. Res.*, 111, D07111.

Le Barbé, L., T. Lebel, and D. Tapsoba, 2002. Rainfall variability in West Africa during the years 1950-90. *J. Climate*, 15, 187-202.

Lebel, T., F. Delclaux, L. Le Barbé and J. Polcher, 2000: From GCM scales to hydrological scales: rainfall variability in West Africa. *Stoch. Env. Res. Risk*, 14, 275-295.

Mathon, V., H. Laurent and T. Lebel, 2002. Mesoscale convective system rainfall in the Sahel. *J. Appl. Meteor.*, 41, 1081-1092.

Matthews, M., 2004: Intraseasonal variability over tropical Africa during northern summer. *J. Climate*, 17, 2427-2440.

Miller, M. A. and A. Slingo, 2007: The Arm Mobile Facility and its first international deployment: Measuring radiative flux divergence in West Africa. *Bull. Amer. Meteor. Soc.*, 88, 1229-1244.

Nuret, M., J.P Lafore, O. Bock, F. Guichard, A. Agusti-Panareda, J.-B. N'Gamini and J.-L. Redelsperger, 2007: Correction of humidity bias for Vaisala RS80 sondes during AMMA 2006 Observing Period, *J. Atmos. Ocean Tech.*, early online release. [DOI: 10.1175/2008JTECHA1103.1]

Parker, D. J., C. D. Thorncroft, R. R. Burton and A. Diongue-Niang, 2005: Analysis of the African easterly jet, using aircraft observations from the JET2000 experiment. *Quart. J. Roy. Meteor. Soc.*, 131, 1461-1482.

Parker, D. J., Fink, A., Janicot, S., Ngamini, J.-B., Douglas, M., Afiesimama, E., Agusti-Panareda, A., Beljaars, A., Dide, F., Diedhiou, A., Lebel, T., Polcher, J., Redelsperger, J.-L., Thorncroft, C., Wilson, G. A., 2008. The AMMA radiosonde program and its implications for the future of atmospheric monitoring over Africa. *Bull. Amer. Meteor. Soc.*, 89, 1015-1027.

Peyrille, P., J.-P. Lafore, and J.-L. Redelsperger, 2007: An idealized two-dimensional framework to study the West African monsoon. Part I: validation and key controlling factors. *J. Atmos. Sci*., 64, 2765-2782.

Ramel, R., H Gallée and C. Messager, 2006: On the northward shift of the West African monsoon. *Clim. Dyn.*, 26, 429–440.

Reed, R.J., D.C. Norquist and E.E. Recker, 1977. The structure and properties of African wave disturbances as observed during Phase III of GATE. *Mon. Wea. Rev.*, 105, 317-333.

Redelsperger, J.-L., Thorncroft, C., Diedhiou, A., Lebel, T., Parker, D. J., Polcher, J., 2006. African Monsoon Multidisciplinary Analysis (AMMA): An international research project and field campaign. *Bull. Amer. Meteor. Soc.*, 87, 1739-1746.

Samain O., L. Kergoat, P. Hiernaux, F. Guichard, E. Mougin, F. Timouk, and F. Lavenu, 2008: Analysis of the in-situ and MODIS albedo variability at multiple time scales in the Sahel, *J. Geophys. Res.*, 113, D14119, doi:10.1029/2007JD009174, 2008.

Siebesma, A. P., C. Jakob, G. Lenderink, R. A. J. Neggers, J. Teixeira, E. van Meijgaard, J. Calvo, A. Chlond, H. Grenier, C. Jones, M. Kohler, H. Kitagawa, P. Marquet, A. P. Lock, F. Muller, D. C. Olmeda and C. Severijns, 2004: Cloud representation in general-circulation models over the northern Pacific Ocean: A EUROCS intercomparison study. *Quart. J. Roy. Meteor. Soc.*, 130, 3245–3267.

Söhne, N., J.-P. Chaboureau and F. Guichard, 2008: Verification of cloud cover forecast with satellite observation over West Africa, *Mon. Wea. Rev*., early online release. [DOI: 10.1175/2008MWR2432.1]

Sultan B. and S. Janicot, 2003. The West African monsoon dynamics. Part II: the "preonset" and "onset" of the summer monsoon. *J. Climate*, 16, 3389-3406.

Taylor, C. M., Lebel, T., 1998. Observational evidence of persistent convective-scale rainfall patterns. *Mon. Wea. Rev.*, 126, 1597–1607.

Taylor C. M., D. B. Clark, 2001: The diurnal cycle and African easterly waves: A land surface perspective. *Quart. J. Roy. Meteor. Soc.,* 127, 845-867.

Taylor, C. M., E. F. Lambin, N. Stephenne, R. J. Harding and R. L. H. Essery, 2002: The influence of land use change on climate in the Sahel. *J. Climate*, 15, 3615-3629.

Thorncroft, C. D., and M. Blackburn, 1997: On the maintenance of the African Easterly Jet. *Quart. J. Roy. Meteor. Soc.*, 123, 763-786.

Thorncroft, C. D., and K. Hodges, 2001: African easterly wave variability and its relationship to Atlantic tropical cyclone activity. *J. Climate*, 14, 1166-1179.

Thorncroft, C.D., D. J. Parker, R. R. Burton, M. Diop, J. H. Ayers, H. Barjat, S. Devereau, A. Diongue, R. Dumelow, D. R. Kindred, N. M. Price, M. Saloum, C. M. Taylor, and A. M. Tompkins, 2003: The JET2000 project: aircraft observations of the African easterly jet and African easterly waves. *Bull. Amer. Meteor. Soc.,* 84, 337–351.

Tompkins A. M., C. Cardinali, J.-J. Morcrette and M. Rodwell, 2005: Influence of aerosol climatology on forecasts of the African Easterly Jet. *Geophys. Res. Lett.*, 32, L10801.

Xue, Y., K.-M. Lau, K. H. Cook, D. Rowell, A. Boone, J. Feng, T. Bruecher, F. De Sales, P. Dirmeyer, L. M. Druyan, A. Fink, M. Fulakeza, Z. Guo, S. M. Hagos, S. S. Ibrah, K.-M. Kim, A. Kitoh, A. Konare, V. Kumar1, P. Lonergan, M. Pasqui1, I. Poccard-Leclercq, N. Mahowald, W. Moufouma-Okia, P. Pegion, J. K. Schemm, S. D. Schubert, A. Sealy, W. M. Thiaw, A. Vintzileos, E. K. Vizy, S. Williams, M.-L. C. Wu, 2008a: The West African Monsoon Modeling and Evaluation project (WAMME) and its First Model Intercomparison Experiment. submitted to *Bull. Amer. Meteor. Soc.*

Xue, Y., P. M. Ruti, A. Boone and F. Hourdin, 2008b: West African monsoon and its modeling. submitted to *Bull. Amer. Meteor. Soc*.

Zheng, X. and E. A. B. Eltahir, 1998. A soil moisture–rainfall feedback mechanism, 2, Numerical experiments. *Water Resour. Res.*, 34, 777–785.